processes

MDPI

Article

Response Surface Methodology for Modelling and Optimization of Chromium Adsorption onto Magnetic Carbon Nanocomposites

Jasmina Nikić, Marko Šolić, Aleksandra Kulić Mandić, Jovana Pešić Bajić, Minja Bogunović Koljaja, Malcolm Watson * and Jasmina Agbaba

Department of Chemistry, Biochemistry and Environmental Protection, University of Novi Sad Faculty of Sciences, Trg Dositeja Obradovića 3, 21000 Novi Sad, Serbia; jasmina.nikic@dh.uns.ac.rs (J.N.); marko.solic@dh.uns.ac.rs (M.Š.); aleksandra.kulic@dh.uns.ac.rs (A.K.M.); jovana.pesic@dh.uns.ac.rs (J.P.B.); minja.bogunovic@dh.uns.ac.rs (M.B.K.); jasmina.agbaba@dh.uns.ac.rs (J.A.)
* Correspondence: malcolm.watson@dh.uns.ac.rs

Abstract

Magnetic carbon nanocomposites are promising adsorbents for toxic metal removal owing to their adsorption capacity and facile magnetic separation. In this study, Response Surface Methodology (RSM) using a Box–Behnken design was applied to investigate and optimize chromium removal from initially Cr(VI)-containing solutions using magnetic activated carbon (MAC) and magnetic biochar (MBC). The effects of pH, initial Cr(VI) concentration, adsorbent dose, and contact time were evaluated using quadratic regression models and analysis of variance (ANOVA). The RSM models were statistically significant for both adsorbents, with a stronger goodness-of-fit for MAC (R^2 = 0.929, adjusted R^2 = 0.835) than for MBC (R^2 = 0.846, adjusted R^2 = 0.640). For MAC, the largest fitted contributions were associated with initial Cr(VI) concentration and adsorbent dose, whereas the MBC response was more strongly associated with initial Cr(VI) concentration and contact time, including a significant pH × contact time interaction. Numerical optimization identified a model-predicted high-removal region for MAC at pH 5.33, an initial Cr(VI) concentration of 0.10 mg L^{-1}, an adsorbent dose of 2.00 g L^{-1}, and a contact time of 120.3 min, whereas the model-predicted maximum for MBC occurred at the boundary of the experimental domain. Random Forest and Support Vector Regression were additionally evaluated using leave-one-out cross-validation. For MAC, Random Forest yielded the numerically highest cross-validated performance (R^2 = 0.613), although bootstrap uncertainty analysis did not support a definitive model ranking based on R^2 and RMSE. Cross-validated predictive performance was substantially lower for the MBC dataset. Overall, RSM and machine learning provided complementary information on fitted response patterns, model-based optimization, and cross-validated predictive performance.

Keywords: Response Surface Methodology; chromium; magnetic activated carbon; magnetic biochar; adsorption optimization; ANOVA; machine learning

Check for updates

Academic Editor: Anna Wołowicz

Received: 22 September 2026
Revised: 26 October 2026
Accepted: 28 October 2026
Published: 31 October 2026

Copyright: © 2026 by the authors. Licensee MDPI, Basel, Switzerland. This article is an open access article distributed under the terms and conditions of the Creative Commons Attribution (CC BY) license.

1. Introduction

Water pollution caused by toxic heavy metals remains one of the most pressing environmental and public health challenges worldwide [1]. The unchecked expansion of industrial activities, coupled with increasing anthropogenic pressures, has profoundly altered the quality of aquatic ecosystems, resulting in the widespread dissemination of

toxic metals in natural water resources [2,3]. Due to their persistence, non-biodegradability, and tendency to bioaccumulate within food chains, heavy metals pose severe threats to ecosystems, economic development, and human health [4–6]. Among these pollutants, chromium has emerged as a contaminant of particular environmental concern owing to its extensive use in numerous industrial sectors, including electroplating, leather tanning, metallurgy, textile manufacturing, pigment production, and mining activities [2,7]. The extensive industrial utilization of chromium, together with inadequate wastewater treatment and disposal practices, has resulted in elevated chromium concentrations in natural water bodies, thereby intensifying concerns regarding water quality and environmental sustainability [8].

Hexavalent chromium (Cr(VI)) represents the most toxic and mobile chromium species [9,10]. Its high solubility and strong oxidizing nature facilitate its transport through aquatic environments and biological membranes, leading to significant health risks for humans and other living organisms [7,11]. Long-term exposure to Cr(VI) has been associated with oxidative stress, liver and kidney dysfunction, respiratory diseases, genetic damage, cardiovascular disorders, infertility, bone abnormalities, and various forms of cancer [6,11]. Owing to these serious adverse effects, regulatory agencies such as the World Health Organization (WHO) and the United States Environmental Protection Agency (US EPA) have established strict limits for chromium concentrations in drinking water, typically set at 0.05 mg/L, highlighting the urgent need for efficient and sustainable remediation technologies [12]. Rapid industrialization and the growing demand for clean water have intensified concerns regarding chromium contamination. In many regions, insufficient wastewater treatment infrastructure and inadequate regulations governing industrial discharges further aggravate the problem, increasing the risk of future water scarcity. Consequently, the development of cost-effective and environmentally friendly treatment strategies capable of efficiently removing Cr(VI) from contaminated waters has become a major research priority.

Various physicochemical and biological approaches, including chemical precipitation, ion exchange, membrane filtration, electrochemical reduction, bioremediation, and photocatalysis, have been extensively investigated for the removal of chromium from contaminated waters [13,14]. Despite their demonstrated effectiveness, many of these technologies are hindered by inherent limitations, such as high operational and maintenance costs, incomplete contaminant removal, excessive sludge generation, membrane fouling, and complex process requirements, which restrict their large-scale implementation [15]. Consequently, adsorption has emerged as one of the most attractive and versatile treatment strategies owing to its operational simplicity, high removal efficiency, cost-effectiveness, and the possibility of adsorbent regeneration and reuse [16,17]. In response to the growing demand for sustainable water treatment technologies, considerable research efforts have been devoted to the development of novel adsorbent materials exhibiting enhanced adsorption capacity, selectivity, stability, and recyclability [18].

Among the diverse classes of adsorbents, magnetic carbon-based nanocomposites have attracted considerable scientific interest because they combine the high specific surface area, well-developed porous structure, and tunable surface chemistry of carbonaceous materials with the magnetic properties of iron oxide nanoparticles [19,20]. The synergistic interaction between these components not only enhances adsorption performance by increasing the availability of active adsorption sites but also enables the rapid and efficient separation of the adsorbent from treated water by means of an external magnetic field [3,9,11,21]. Consequently, these hybrid materials facilitate post-treatment recovery and regeneration while minimizing secondary pollution, thereby improving the overall sustainability of the adsorption process. Owing to these advantageous physicochemical and magnetic properties,

magnetic activated carbon, magnetic biochar, graphene-based composites, and other iron oxide-functionalized carbon materials have emerged as promising candidates for Cr(VI) remediation, exhibiting high adsorption capacities and excellent removal efficiencies in aqueous systems [3,7,9,11,22,23].

In addition to the development of highly efficient adsorbent materials, the optimization of operating conditions plays a pivotal role in maximizing adsorption performance while minimizing chemical consumption and operational costs. Response Surface Methodology (RSM) is a statistical and mathematical technique widely employed to analyse and model the relationships between independent variables and the corresponding process responses [24]. The primary objective of RSM is to establish a functional relationship between process parameters and system performance, while simultaneously identifying the optimal operating conditions. Compared with conventional one-factor-at-a-time (OFAT) approaches, RSM enables the simultaneous evaluation of multiple process variables and their interactions, thereby reducing the number of experiments required and improving the efficiency of the optimization process. A major advantage of RSM lies in its ability to identify interaction effects among factors, which are often overlooked by traditional OFAT experiments, thus providing a more comprehensive understanding of the relationships governing the investigated system [25].

In practice, adsorption systems are commonly described using second-order polynomial models, which are capable of capturing both nonlinear effects and interactions among process variables. The adequacy of the developed models is typically assessed by analysis of variance (ANOVA), residual diagnostics, and goodness-of-fit statistics, whereas the response behaviour is visualized through three-dimensional response surfaces and contour plots [26]. Owing to its ability to provide comprehensive information with relatively low experimental effort, RSM has been extensively applied to optimize Cr(VI) adsorption processes [9,10,22]. Among the experimental designs employed in RSM, Central Composite Design (CCD) and Box–Behnken Design (BBD) are the most frequently used for the development of quadratic predictive models. Compared with CCD, BBD avoids extreme combinations of factors and requires a smaller number of experiments while maintaining the ability to evaluate linear, quadratic, and interaction effects [24]. Owing to its statistical efficiency and reduced experimental cost, BBD has been extensively applied to optimize Cr(VI) adsorption processes and other environmental applications [25,27,28].

More recently, advances in artificial intelligence have stimulated growing interest in the application of machine-learning algorithms to environmental systems. Techniques such as Artificial Neural Networks (ANN), Random Forest (RF), and Support Vector Regression (SVR) have demonstrated considerable potential for predicting adsorption behaviour and identifying the key parameters governing contaminant removal. These approaches are particularly attractive because they can capture complex nonlinear relationships among operational variables that are often difficult to describe using conventional mathematical models.

Among the available algorithms, Random Forest (RF) and Support Vector Regression (SVR) have attracted increasing attention because of their ability to capture complex nonlinear relationships among process variables without imposing predefined functional forms. Owing to these characteristics, both algorithms have been increasingly applied to model adsorption processes involving heavy metals and dyes.

Recent studies have demonstrated the combined use of response-surface methodology and machine-learning approaches for Cr(VI) adsorption, including magnetic adsorbent systems [22]. Building on this developing literature, the present study focuses on the direct comparison of magnetic activated carbon (MAC) and magnetic biochar (MBC) under the same experimental design, with particular attention to the response patterns of the two

materials and the relationship between model-based factor effects and data-driven variable rankings. The same MAC and MBC materials were previously characterized and evaluated for arsenic removal [20], while their behaviour toward Cr(VI) under systematically varied operating conditions has not been explored within a common response-surface and machine-learning framework.

Accordingly, the objective of the present study was to investigate and optimize chromium removal from initially Cr(VI)-containing solutions using MAC and MBC through Response Surface Methodology (RSM) based on a Box–Behnken experimental design. The effects of solution pH, initial Cr(VI) concentration, adsorbent dosage, and contact time on chromium removal efficiency were systematically investigated. In addition, Random Forest (RF) and Support Vector Regression (SVR) were applied as complementary data-driven approaches and evaluated alongside the RSM models. Feature-importance analysis was used to explore the relative contribution of the investigated process variables and to descriptively compare the resulting rankings with the factor effects obtained from the statistical analysis.

2. Experimental

2.1. Materials and Methods

All chemicals used in this study were of analytical grade and were used as received without further purification. A stock solution of Cr(VI) (1000 mg L^{-1}) was prepared by dissolving potassium dichromate ($K_2Cr_2O_7$, Sigma-Aldrich(Merck KGaA, Darmstadt, Germany), analytical grade) in deionized water. Working solutions of the desired chromium concentrations were freshly prepared by appropriate dilution of the stock solution prior to each adsorption experiment. The pH of the solutions was adjusted using 0.1 M sodium hydroxide (NaOH, Sigma-Aldrich, analytical grade) or 0.1 M nitric acid (HNO_3, Fluka (Seelze, Germany), analytical grade). All aqueous solutions were prepared with deionized water produced by a laboratory water purification system (LABCONCO WaterPro RO/PS Station, Kansas City, MO, USA), meeting ASTM Type I specifications (conductivity 0.55 μS cm^{-1}; TOC < 0.5 mg C L^{-1}).

The magnetic activated carbon (MAC) and magnetic biochar (MBC) used in the present experiments were synthesized by the co-precipitation procedure described in our previous study [20]. The same material batches characterized in that work were used in the present study. XRD analysis confirmed the incorporation of a spinel-type iron oxide phase assigned to magnetite, while FTIR spectra showed characteristic Fe–O bands at approximately 628–630 and 586 cm^{-1}. SEM/EDS analysis confirmed substantial iron incorporation, with Fe contents of 57.2 wt.% for MAC and 70.3 wt.% for MBC. The specific surface areas of MAC and MBC were 193.9 and 116.3 m^2 g^{-1}, respectively; the corresponding micropore volumes were 0.039 and 0.006 cm^3 g^{-1}, mesopore volumes were 0.282 and 0.260 cm^3 g^{-1}, and average pore sizes were 6.89 and 9.76 nm. The previously determined pHpzc values were 6.57 for MAC and 6.36 for MBC [20]. Post-adsorption characterization is not included in the present manuscript, which focuses on response-surface and machine-learning analysis of chromium removal from initially Cr(VI)-containing solutions. These data are being considered together with dedicated equilibrium-isotherm and kinetic experiments in a separate mechanistic study. Consequently, physicochemical characteristics reported here are used as material context and not as direct evidence of the Cr(VI) adsorption mechanism.

2.2. Batch Adsorption Experiment

Batch adsorption experiments were performed according to the experimental matrix generated by the Box–Behnken design (Table 1). For each experimental run, 30 mL of the prepared Cr(VI) solution was transferred into a glass vial. Depending on the experimental design, the adsorbent dosage varied between 0.2 and 2.0 g L^{-1}, the solution pH ranged

from 5 to 9, the initial Cr(VI) concentration from 0.10 to 100 mg L^{-1}, and the contact time from 20 to 240 min. The pH range of 5–9 was selected to investigate chromium removal under moderately acidic to moderately alkaline conditions, considering both the physicochemical properties of the adsorbents and the potential relevance of these conditions to water treatment applications. This interval encompasses the previously determined points of zero charge of MAC (6.57) and MBC (6.36) [20], allowing the adsorption response to be evaluated below and above these characteristic values. Furthermore, the selected range covers the pH-dependent shift in Cr(VI) speciation from predominantly $HCrO_4^-$ toward CrO_4^{2-}. The relevance of investigating Cr(VI) adsorption under such conditions is also supported by Javid et al. (2020) [29], who reported favourable adsorption near neutral pH using an RSM-based approach. From a practical perspective, operation under strongly acidic conditions may require additional acid dosing and subsequent pH adjustment, potentially increasing chemical consumption and operational complexity [30]. Although strongly acidic conditions may enhance Cr(VI) adsorption, they were outside the scope of the present experimental design. Accordingly, the reported optimization results are restricted to the investigated pH range. The initial Cr(VI) concentration range (0.10–100 mg L^{-1}) was selected to provide a broad concentration domain for response-surface analysis. However, because the Box–Behnken design used linearly spaced factor levels, the trace-concentration region is represented only at the lower boundary of the design. Therefore, the present experimental design provides limited resolution of adsorption behaviour in the trace-concentration range.

Table 1. Actual and coded levels of the independent variables used in the Box–Behnken experimental design.

Factors	Unit	Levels		
Coded levels		−1	0	+1
Solution pH		5	7	9
Initial Cr (VI) concentration	mg L^{-1}	0.10	50.1	100
Adsorbent dose	g L^{-1}	0.2	1.1	2
Contact time	min	20	130	240

The suspensions were agitated at 180 rpm at room temperature using an orbital shaker. After the predetermined contact time, the adsorbent was separated from the solution using an external magnet. Chromium concentrations in the aqueous phase were determined by inductively coupled plasma mass spectrometry (ICP-MS; Agilent 7700 Series, Tokyo, Japan) according to US EPA Method 6020B [31]. A multi-element standard (CPAChem, Stara Zagora, Bulgaria) was used for calibration over the range of 0.001–2 mg L^{-1}. Given the wide range of initial chromium concentrations investigated (up to 100 mg L^{-1}), initial solutions were diluted as necessary (by 50 for the highest concentrations) to ensure that concentrations fell within the analytical calibration range (up to 2 mg L^{-1}). Treated samples were initially analysed without dilution and, where measured concentrations exceeded the calibration range, were diluted as necessary and reanalysed. In all cases, the measured concentrations were corrected using the corresponding dilution factors to obtain the final chromium concentrations in the undiluted samples. The ^{52}Cr isotope was monitored, and analyses were performed in helium collision mode to minimize polyatomic interferences. The method detection limit (MDL) and limit of quantification (LOQ) for chromium were 0.0010 and 0.0031 mg L^{-1}, respectively. Initial calibration verification and continuing calibration verification were used as quality-control checks. No internal standard was applied. Instrument drift was instead monitored via the response of the calibration verification standard, which was analysed in the run every 10 samples.

Prior to analysis, samples were filtered and preserved at pH < 2 using trace-metal-grade nitric acid. ICP-MS quantified total chromium in the filtered aqueous phase and did not distinguish between Cr(VI) and Cr(III). Since the initial solutions were prepared from $K_2Cr_2O_7$, chromium was initially present as Cr(VI); however, possible changes in oxidation state during contact with the adsorbents were not determined.

Accordingly, the experimental response is reported as total chromium removal according to Equation (1):

$$\text{Removal } (\%) = \frac{C_0 - C_t}{C_0} \times 100 \quad (1)$$

where C_0 is the initial chromium concentration in the solution prepared from Cr(VI), and C_t is the residual total chromium concentration in the aqueous phase measured after the specified contact time (mg L^{-1}).

In addition to removal efficiency, the experimental chromium uptake, q_t, was calculated according to Equation (2):

$$q_t \left(\text{mg } g^{-1}\right) = (C_0 - C_t) \times V/m \quad (2)$$

where q_t is the chromium uptake at the specified contact time (mg g^{-1}), (V) is the solution volume (L), and (m) is the adsorbent mass (g). Because q_t was strictly positive and covered a wide numerical range, a complementary response-metric sensitivity analysis was performed using $\ln(q_t)$ as the response. The same full hierarchical quadratic model and block structure used for removal efficiency were retained. Fitted values were back-transformed to the original (q_t) scale using a smearing correction. This analysis was intended to assess the sensitivity of factor interpretation to the selected response metric rather than to replace removal efficiency as the primary response.

2.3. Experimental Design and Statistical Analysis

A four-factor, three-level Box–Behnken experimental design (BBD) consisting of 29 experimental runs was generated using Design-Expert® software (Version 13, Stat-Ease Inc., Minneapolis, MN, USA). The design comprised 24 edge-midpoint runs and five centre-point runs. The experiments were conducted on the same day in three sequential experimental series, which were treated as blocks in the statistical model for practical organization of the experimental runs. The three blocks contained 10, 10, and 9 runs, respectively, and the five centre-point runs were distributed across the blocks as 2, 2, and 1 replicates. Blocking was included to account for potential between-series variability unrelated to the investigated process factors. The investigated independent variables were solution pH, initial Cr(VI) concentration, adsorbent dose and contact time, while chromium removal efficiency (%) was selected as the response variable. Each factor was evaluated at three coded levels (−1, 0, and +1), corresponding to the lower, central, and upper values of the selected experimental range. The actual and coded levels of the investigated variables are summarized in Table 1. To minimize the influence of uncontrolled experimental factors, all experimental runs were performed in a randomized order. The experimental design enabled the simultaneous evaluation of the linear, quadratic, and interaction effects of the investigated variables while minimizing the total number of experimental runs required.

Statistical analyses were performed using Python 3.14 (Python Software Foundation, Wilmington, DE, USA) within the PyCharm 2026.1.2 integrated development environment (JetBrains, Prague, Czech Republic). Response Surface Methodology (RSM) was implemented by fitting second-order polynomial regression models to the experimental data using the statsmodels package. The relationship between the investigated pro-

cess variables and chromium removal efficiency was described by the following quadratic polynomial equation:

$$Y = \beta_0 + \sum_{i=1}^{k} \beta_i X_i + \sum_{i=1}^{k} \beta_{ii} X_i^2 + \sum_{i<j}^{k} \beta_{ij} X_i X_j \quad (3)$$

where Y is the predicted chromium removal efficiency, β_0 is the intercept, β_i are the linear regression coefficients, β_{ii} are the quadratic coefficients, β_{ij} are the interaction coefficients, and X_i and X_j represent the coded independent variables.

The statistical significance of the developed models and individual regression terms was evaluated by analysis of variance (ANOVA) at a 95% confidence level ($p < 0.05$). The full hierarchical quadratic model was retained for both adsorbents irrespective of the statistical significance of individual terms in order to preserve model hierarchy and the pre-specified second-order response-surface structure of the Box–Behnken design. No stepwise term selection was performed. Given the number of coefficients evaluated within each model, individual term-wise p-values were interpreted as nominal evidence, and values close to the $p = 0.05$ threshold were interpreted cautiously. Model adequacy was assessed using the coefficient of determination (R^2), adjusted coefficient of determination (Adj. R^2), Akaike Information Criterion (AIC), Bayesian Information Criterion (BIC), predicted-versus-observed plots, residual-versus-predicted plots, normal probability (Q–Q) plots, Cook's distance, leverage values, studentized residuals, and Pareto charts of standardized effects. Numerical optimization was performed by maximizing the model-predicted chromium removal efficiency while constraining all process variables within the investigated experimental ranges.

To complement the RSM analysis, Random Forest (RF) and Support Vector Regression (SVR) were implemented using the scikit-learn library as exploratory data-driven models. Owing to the small experimental dataset ($n = 29$), model performance was evaluated using a common leave-one-out cross-validation (LOOCV) framework rather than a single training/test split. In each LOOCV iteration, one experimental observation was withheld for validation and the remaining observations were used for model fitting. Model performance was summarized using R^2, RMSE, and MAE. For SVR, feature standardization was performed within each training fold using a Pipeline to avoid information leakage. The machine-learning analysis was intended as a complementary exploratory assessment rather than as evidence of broadly generalizable predictive models.

The Random Forest model comprised 200 trees (n_estimators = 200) and used a fixed random seed (random_state = 42) to ensure reproducibility. The remaining Random Forest hyperparameters were left at the scikit-learn default settings, including unrestricted tree depth (max_depth = None) and a minimum of one sample per leaf (min_samples_leaf = 1). The SVR model employed a radial basis function (RBF) kernel with C = 100, gamma = 'scale', and $\varepsilon = 0.1$. No automated hyperparameter tuning was performed; the same model settings were retained throughout the LOOCV procedure. Uncertainty in the LOOCV performance estimates was assessed using 10,000 paired bootstrap resamples of the observed responses and corresponding out-of-fold predictions (random seed = 42). Bootstrap 95% confidence intervals were calculated for individual performance metrics and for pairwise differences between models.

Model performance was quantified using the coefficient of determination (R^2), root mean square error (RMSE), and mean absolute error (MAE), calculated according to Equations (4)–(6), respectively.

$$R^2 = 1 - \frac{\sum_{i=1}^{n} (y_i - \hat{y}_i)^2}{\sum_{i=1}^{n} (y_i - \overline{y})^2} \quad (4)$$

$$RMSE = \sqrt{\frac{1}{n}\sum_{i=1}^{n}(y_i - \hat{y}_i)^2} \quad (5)$$

$$MAE = \frac{1}{n}\sum_{i=1}^{n} | y_i - \hat{y}_i | \quad (6)$$

where y_i represents the experimental value, $\hat{y}_i$ is the predicted value, $\overline{y}$ is the mean of the experimental values, and n is the total number of observations.

In addition, Random Forest feature-importance analysis was performed to assess the relative contribution of individual input variables to the fitted predictive model. Feature importance was quantified using the impurity-based measure. For the detailed analysis reported for MAC, the Random Forest model was fitted to the complete dataset using 200 trees and repeated across 30 random seeds to assess the stability of the variable ranking. Mean feature importance, standard deviation, mean rank, and the frequency with which each variable was ranked first were calculated across the repeated fits. The resulting ranking was considered qualitatively alongside the RSM results. Because Random Forest feature importance and ANOVA statistics quantify different aspects of variable influence, their numerical values were not treated as directly comparable measures. Feature-importance values were interpreted as contributions of the input variables to the fitted Random Forest model rather than as measures of statistical significance or causal effects on the adsorption process.

Data preprocessing was performed using the pandas library, numerical computations were carried out with NumPy, and graphical visualization was generated using Matplotlib version 3.10.9.

3. Results and Discussion

3.1. Model Adequacy and Analysis of Variance (ANOVA)

Response Surface Methodology (RSM) was employed to develop second-order polynomial models describing the influence of solution pH, initial Cr(VI) concentration, adsorbent dose, and contact time on chromium removal by MAC and MBC. The experimental conditions and corresponding experimental and predicted chromium removal efficiencies for MAC and MBC are presented in Table S1 (Supplementary Materials). The goodness-of-fit and statistical adequacy of the developed models were evaluated using the coefficient of determination (R^2), adjusted coefficient of determination (Adj. R^2), F-value, model significance (p-value), and the Akaike (AIC) and Bayesian (BIC) information criteria. The corresponding statistical indicators are summarized in Table 2.

Table 2. Statistical indicators of the developed quadratic response surface models for chromium adsorption onto MAC and MBC.

Parameter	MAC	MBC
R^2	0.929	0.846
Adjusted R^2	0.835	0.640
AIC	232.5	183.2
AICc	288.1	238.9
BIC	255.7	206.4
F-value	9.881	4.116
Model p-value	0.000137	0.00862

Note: AIC, AICc, and BIC are reported as model-specific information criteria and were not used for direct comparison between the MAC and MBC models because the models describe different response datasets.

The developed quadratic response surface models were statistically significant for both adsorbents; however, their predictive performances differed considerably. The MAC model exhibited excellent goodness-of-fit, with a coefficient of determination of $R^2 = 0.929$ and an adjusted coefficient of determination of Adj. $R^2 = 0.835$, indicating that approximately 92.9% of the variability in chromium removal was explained by the developed quadratic model. Furthermore, the model was highly significant ($F = 9.881$, $p = 0.000137$), confirming that the selected second-order polynomial adequately described the relationship between the investigated process variables and chromium removal efficiency within the studied experimental domain.

The MBC model was likewise statistically significant ($F = 4.116$, $p = 0.00862$), although it exhibited a weaker goodness-of-fit than the MAC model, with $R^2 = 0.846$ and Adj. $R^2 = 0.640$. These results indicate that the developed model explained approximately 84.6% of the experimental variability, while the lower adjusted coefficient of determination suggests reduced goodness-of-fit after accounting for the number of model terms. AIC, AICc, and BIC were calculated for each fitted model as model-specific information criteria. Because the MAC and MBC models were fitted to different response datasets, these criteria were not used for direct comparison between the two adsorbents. Accordingly, the higher R^2 and adjusted R^2 values obtained for MAC indicate that its quadratic response surface model provided a stronger representation of the observed experimental response than the corresponding MBC model. These statistics characterize model fit to the available data and should not be interpreted as evidence of superior out-of-sample predictive performance. Out-of-sample performance was evaluated separately using the common LOOCV framework described in Section 3.4. The ANOVA results (Tables 3 and 4) further revealed distinct differences in the contribution of the investigated process variables to chromium removal by the two adsorbents. For MAC, the linear effects of the initial Cr(VI) concentration ($F = 73.314$, $p < 0.0001$) and adsorbent dose ($F = 17.574$, $p = 0.0012$) were statistically significant, whereas the linear effects of solution pH and contact time were not statistically significant ($p > 0.05$). These results indicate that the fitted MAC response was most strongly associated with initial Cr(VI) concentration and adsorbent dose within the investigated experimental domain. The strong concentration effect is consistent with its role in determining the concentration gradient available for mass transfer, whereas the dose effect is consistent with changes in the amount of adsorbent available to interact with chromium. These interpretations provide physicochemical context for the observed statistical effects but do not constitute direct mechanistic evidence.

The lack-of-fit test for the MAC model was not statistically significant ($F = 5.403$, $p = 0.166$), indicating no statistically detectable lack of fit within the investigated design space. However, this result should be interpreted cautiously because the pure-error estimate was based on a limited number of replicated observations.

For MAC, all four quadratic terms (pH^2, $concentration^2$, $dose^2$, and $contact\ time^2$) had nominal p-values below 0.05 within the fitted full quadratic model, providing evidence of curvature in the response surface. The $dose^2$ ($p = 0.0210$) and $contact\text{-}time^2$ ($p = 0.0148$) effects were interpreted cautiously in view of the number of model terms evaluated. Collectively, the quadratic terms indicate that the experimental response was not adequately described by purely linear relationships over the investigated factor ranges.

In contrast, the MBC model exhibited a less pronounced contribution of quadratic terms than the MAC model. Among the linear terms, initial Cr(VI) concentration ($F = 17.317$, $p = 0.001$) and contact time ($F = 14.495$, $p = 0.002$) had nominal p-values below 0.05. Among the quadratic terms, the $contact\text{-}time^2$ term also had a nominal p-value below 0.05 ($F = 6.127$, $p = 0.029$). The pH × contact-time interaction likewise had a nominal p-value below 0.05 ($F = 8.008$, $p = 0.015$), suggesting that the fitted effect of contact time varied across the

investigated pH range. The remaining interaction and quadratic terms did not reach the nominal $p = 0.05$ threshold. Given the number of coefficients evaluated within the full quadratic model, these term-wise results are interpreted cautiously rather than as strong independent evidence of individual effects.

Table 3. Analysis of variance (ANOVA) for the quadratic response surface model describing chromium adsorption onto MAC.

Source	Sum of Squares (SS)	Df	Mean Square (MS)	F-Value	*p*-Value
Model	20,988.1	16	1311.75	9.881	0.00013
Block	532.500	2	266.2	2.006	0.1772
Linear terms					
pH	302.148	1	302.15	2.276	0.1573
Concentration	9732.368	1	9732.37	73.314	<0.0001
Dose	2332.908	1	2332.91	17.574	0.0012
Contact time	189.721	1	189.72	1.429	0.2550
Quadratic terms					
pH^2	2209.745	1	2209.75	16.646	0.0015
$Concentration^2$	1576.503	1	1576.50	11.876	0.0048
$Dose^2$	935.053	1	935.05	7.044	0.0210
$Contact\ time^2$	1074.008	1	1074.01	8.091	0.0148
Interaction terms					
pH × Concentration	596.269	1	596.27	4.492	0.0556
pH × Dose	693.100	1	693.10	5.221	0.0413
pH × Contact time	118.568	1	118.57	0.893	0.3633
Concentration × Dose	40.230	1	40.23	0.303	0.5921
Concentration × Contact time	99.837	1	99.84	0.752	0.4028
Dose × Contact time	43.004	1	43.00	0.324	0.5797
Residual	1592.986	12	132.749	–	–
Lack-of-Fit	1536.120	10	153.612	5.403	0.166
Pure Error	56.867	2	28.433	–	–
Total	22,581.097	28	–	–	–

The statistical analysis demonstrates that chromium adsorption onto MAC was characterized by stronger nonlinear behaviour and a more complex response surface than that observed for MBC. This is consistent with the higher goodness-of-fit obtained for the MAC model ($R^2 = 0.929$; Adj. $R^2 = 0.835$), indicating that the developed quadratic polynomial more accurately captured the experimental response.

The lack-of-fit test for the MBC model was also not statistically significant ($F = 0.745$, $p = 0.696$), indicating no statistically detectable lack of fit within the investigated design space. As for the MAC model, this result should be interpreted cautiously because the pure-error estimate was based on a limited number of replicated observations.

The replicated centre-point observations also showed appreciable experimental variability. For MBC, the pure-error standard deviation was approximately 5.55%, while the residual RMSE of the fitted model was approximately 4.92%. Thus, the residual variation was of a similar magnitude to the variability observed among the replicated centre points. Given that the pure-error estimate was based on only 2 degrees of freedom, this comparison should be interpreted cautiously; nevertheless, it suggests that experimental repeatability may have contributed substantially to the attainable goodness-of-fit for MBC. For comparison, the corresponding pure-error standard deviation for MAC was approximately 5.33%, whereas its residual RMSE was approximately 11.52%. Accordingly, the weaker

goodness-of-fit of the MBC model should not be attributed to additional unmeasured factors or more complex nonlinear relationships without further evidence.

Table 4. Analysis of variance (ANOVA) for the quadratic response surface model describing chromium adsorption onto MBC.

Source	Sum of Squares (SS)	df	Mean Square (MS)	F-Value	*p*-Value
Model	1597.1	16	99.81	4.116	0.0086
C(Block)	106.4	2	53.22	2.1947	0.154
Linear terms					
pH	40.324	1	40.323	1.663	0.222
Concentration	419.921	1	419.92	17.317	0.001
Dose	27.228	1	27.22	1.123	0.310
Contact time	351.502	1	351.50	14.495	0.002
Quadratic terms					
pH^2	54.065	1	54.06	2.230	0.161
$Concentration^2$	0.183	1	0.1828	0.008	0.932
$Dose^2$	64.995	1	64.99	2.680	0.128
$Contact\ time^2$	148.582	1	148.58	6.127	0.029
Interaction terms					
pH × Concentration	7.479	1	7.479	0.308	0.589
pH × Dose	3.831	1	3.831	0.158	0.698
pH × Contact time	194.203	1	194.20	8.008	0.015
Concentration × Dose	72.585	1	72.58	2.993	0.109
Concentration × Contact time	35.153	1	35.15	1.450	0.252
Dose × Contact time	8.990	1	8.990	0.371	0.554
Residual	290.996381	12	24.24969842		
Lack-of-Fit	229.3807886	10	22.93807886	0.744554356	0.695668247
Pure Error	61.61559243	2	30.80779621		
Total	1888.101	28			

In general, the quadratic model showed a stronger goodness-of-fit for MAC ($R^2 = 0.929$; adjusted $R^2 = 0.835$) than for MBC ($R^2 = 0.846$; adjusted $R^2 = 0.640$). For MAC, all four quadratic terms had nominal *p*-values below 0.05, whereas for MBC the principal fitted contributions were associated with initial Cr(VI) concentration, contact time, the quadratic contact-time term, and the pH × contact-time interaction. These results describe the fitted response structures within the observed dataset and should not be interpreted as evidence that the weaker MBC fit was caused by additional unmeasured factors or more complex mechanisms. Likewise, the goodness-of-fit statistics should not be interpreted as measures of out-of-sample predictive performance, which was evaluated separately using the common LOOCV framework presented in Section 3.4.

To complement the ANOVA results and facilitate interpretation of the developed quadratic models, Pareto charts of standardized effects were generated for both adsorbents (Figure 1).

For MAC, the Pareto chart showed that the linear effect of initial Cr(VI) concentration was the dominant contributor to the fitted response, followed by the linear effect of adsorbent dose and several quadratic terms. Among the interaction terms for MAC, the pH × dose interaction had a nominal *p*-value below 0.05 ($p = 0.0413$), whereas the remaining interactions did not reach this threshold. For MBC, the linear effects of concentration and contact time were the dominant terms, while the pH × contact-time interaction ($p = 0.015$) and the quadratic contact-time term ($p = 0.029$) had nominal *p*-values below 0.05. These

term-wise results are interpreted cautiously because multiple coefficients were evaluated within each full quadratic model. Overall, the ANOVA and Pareto-chart results indicate different fitted response structures for the two adsorbents, with a stronger contribution of quadratic terms for MAC, whereas the MBC response was more strongly associated with concentration and contact time within the investigated design space.

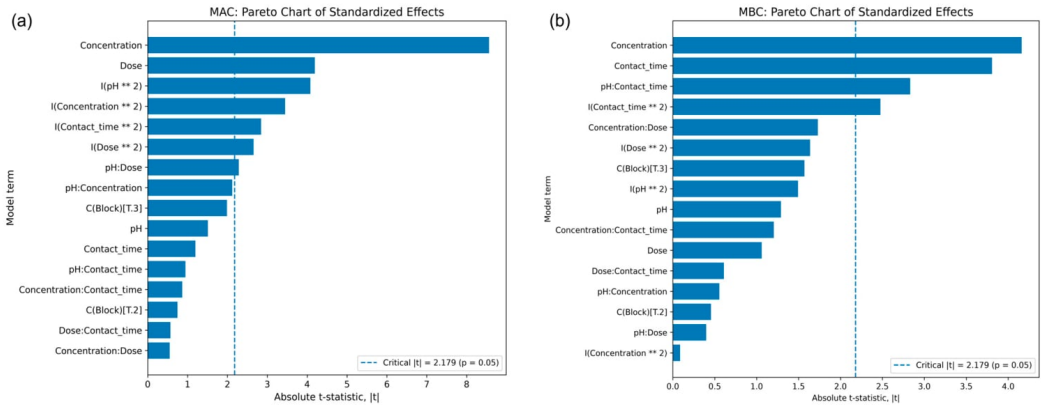


Figure 1. Pareto chart of standardized model effects for chromium removal by (**a**) MAC and (**b**) MBC. Note that ** indicates a squared (second-order) term, i.e. the variable multiplied by itself.

Model validation was performed by examining the agreement between experimental and predicted values together with the residual distribution and normality diagnostics. The predicted versus actual plots (Figure 2a,b) showed satisfactory agreement for both MAC and MBC models, indicating that the developed quadratic equations adequately described the experimental responses within the investigated design space. Consistent with its higher coefficient of determination ($R^2 = 0.929$), the MAC model exhibited a closer clustering of fitted values around the 45° reference line than the MBC model ($R^2 = 0.846$), indicating a better goodness-of-fit to the experimental data. Nevertheless, no pronounced systematic deviations were observed for either adsorbent, indicating that both quadratic models adequately represented the experimental response within the investigated design space. The observed differences between the two models are fully consistent with the ANOVA results, which demonstrated a substantially better fit of the quadratic model for MAC than for MBC. For both adsorbents, the overall block effect was not statistically significant. However, the estimated block coefficients, particularly the positive Block 3 coefficient for MAC, indicate that some between-series variation was present. Therefore, the non-significant block test should be interpreted as insufficient evidence of a systematic block effect rather than as evidence of complete absence of between-block variability. Overall, the agreement between the statistical indicators and graphical diagnostics supports the statistical adequacy of the fitted RSM models for describing the experimental responses within the investigated design space, with a stronger goodness-of-fit observed for MAC.

Visual inspection of the residual-versus-fitted plots (Figure 3a,b) showed no pronounced trend, curvature, or funnel-shaped pattern for either adsorbent, which is consistent with approximately constant residual variance within the observed dataset. Given the limited sample size ($n = 29$), these graphical diagnostics were interpreted as supportive rather than confirmatory evidence regarding model assumptions. No pronounced systematic pattern was apparent in the residual distributions for either model. Residual dispersion was somewhat greater for the MBC model, consistent with its lower coefficient of determination ($R^2 = 0.846$), but the graphical diagnostics did not indicate an obvious systematic departure from the fitted response structure. Overall, these observations support the descriptive adequacy of the fitted models within the investigated experimental design space, with a stronger goodness-of-fit for MAC.

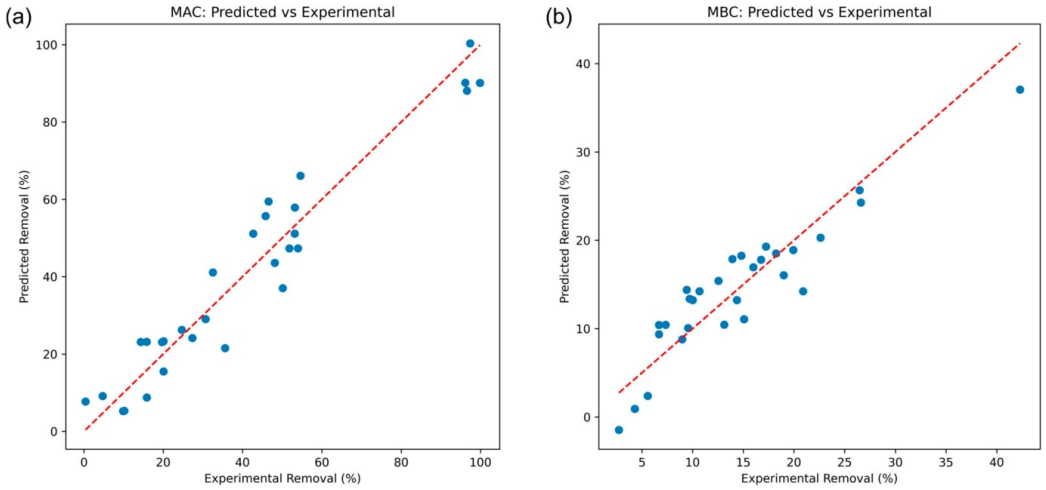


Figure 2. Predicted versus actual chromium removal obtained using the developed RSM models: (**a**) MAC and (**b**) MBC.

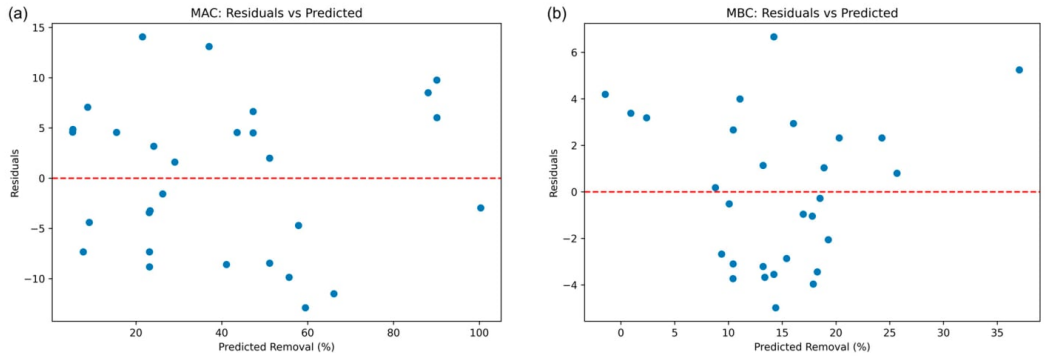


Figure 3. Residuals versus predicted values for chromium removal using (**a**) MAC and (**b**) MBC.

The Q–Q plots (Figure 4) showed approximate alignment of the residuals with the theoretical normal reference line, with minor deviations at the distribution tails. No pronounced departure from normality was evident from visual inspection; however, given the limited sample size ($n = 29$), normality cannot be established conclusively from the graphical diagnostics alone. Accordingly, these plots were used as qualitative diagnostic checks rather than as formal evidence that the distributional assumptions were fully satisfied. The somewhat larger deviation observed for the MBC model is consistent with its greater residual dispersion, but no pronounced systematic departure from the reference line was apparent.

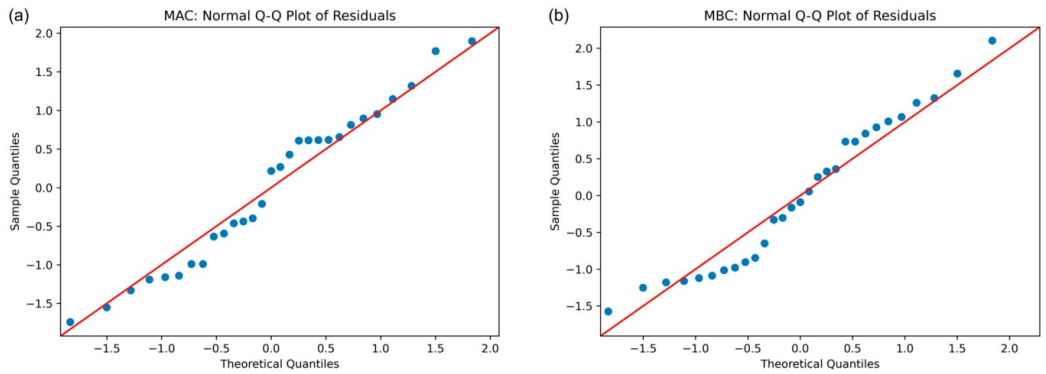


Figure 4. Normal probability (Q-Q) plot of model residuals (**a**) MAC and (**b**) MBC.

Additional influence diagnostics were performed using Cook's distance, studentized residuals, and leverage analysis to evaluate the robustness of the developed quadratic models (Figures 5 and 6). For both adsorbents, several observations exceeded the conservative Cook's distance screening threshold of $4/n$; however, the maximum Cook's distance remained below 1 for both MAC (0.486) and MBC (0.370), indicating that no single observation exerted excessive influence on the fitted models. The externally studentized residuals remained within the conventional ± 3 limits for all observations, with maximum absolute values of 2.493 for MAC and 2.042 for MBC, indicating the absence of substantial outliers. Taken together, these results indicate that the fitted quadratic models were not dominated by individual influential or outlying observations, and all experimental runs were therefore retained in the final regression analysis.

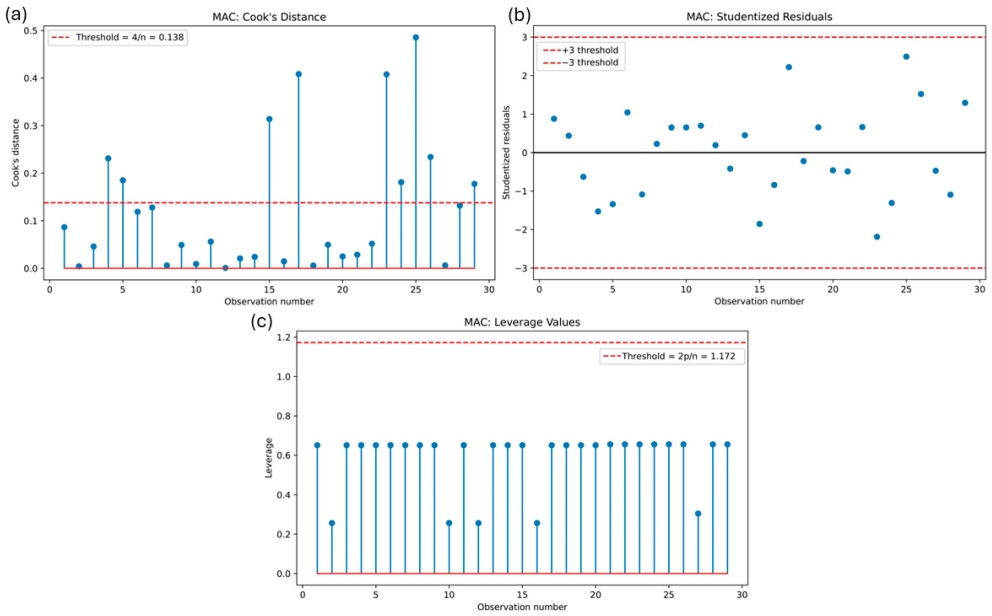


Figure 5. Cook's distance and influence diagnostics for the MAC RSM model: (**a**) Cook's distance; (**b**) studentized residuals; (**c**) leverage values.

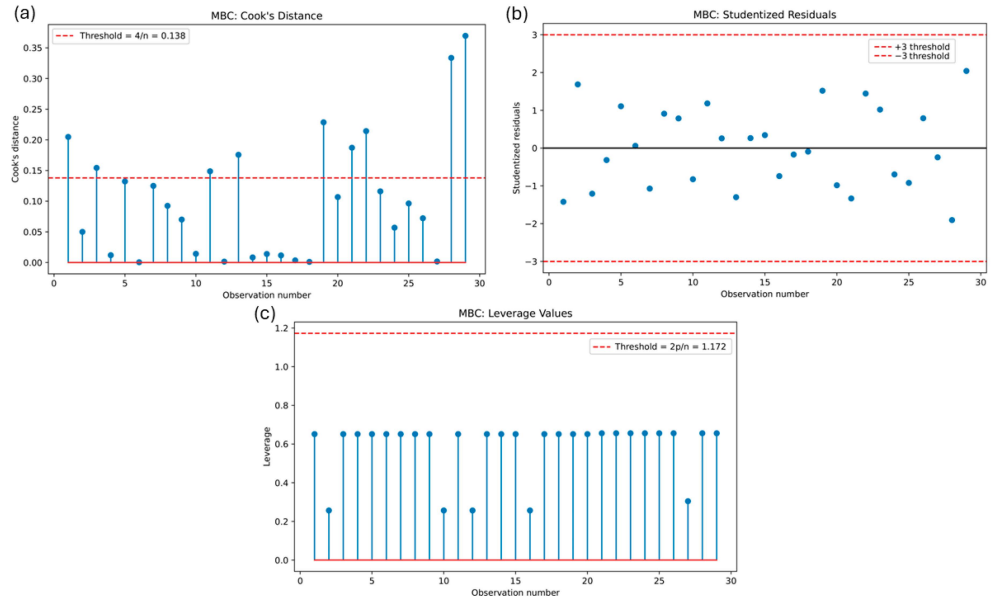


Figure 6. Cook's distance and influence diagnostics for the MBC RSM model: (**a**) Cook's distance; (**b**) studentized residuals; (**c**) leverage values.

The diagnostic plots were used as qualitative checks of model fit and residual behaviour within the observed dataset. No pronounced systematic deviations were evident; however, given the limited sample size (n = 29), these diagnostics do not establish homoscedasticity, normality, or out-of-sample predictive reliability. They therefore provide supportive evidence regarding the descriptive adequacy of the fitted RSM models within the investigated design space, while predictive performance was evaluated separately using LOOCV.

3.2. Effect of Process Variables on Chromium Removal: Response Surface Interpretation

The validated quadratic models were further interpreted using response surface and contour plots to visualize the effects of the investigated process variables on chromium removal. The response surfaces provide insight into the individual and combined influence of solution pH, initial Cr(VI) concentration, adsorbent dose, and contact time on the adsorption performance of MAC and MBC. The effects of each variable are discussed separately below.

3.2.1. Effect of Solution pH on Chromium Removal

Solution pH is an important factor affecting chromium removal from initially Cr(VI)-containing solutions, as it influences chromium speciation and the surface charge of the adsorbent [18].

Within the investigated pH range, the calculated distribution of Cr(VI) species in the initial solutions shifts from $HCrO_4^-$ toward CrO_4^{2-} as pH increases (Figure 7) [32], while changes in surface protonation may influence interactions between the adsorbents and Cr(VI) species [33].

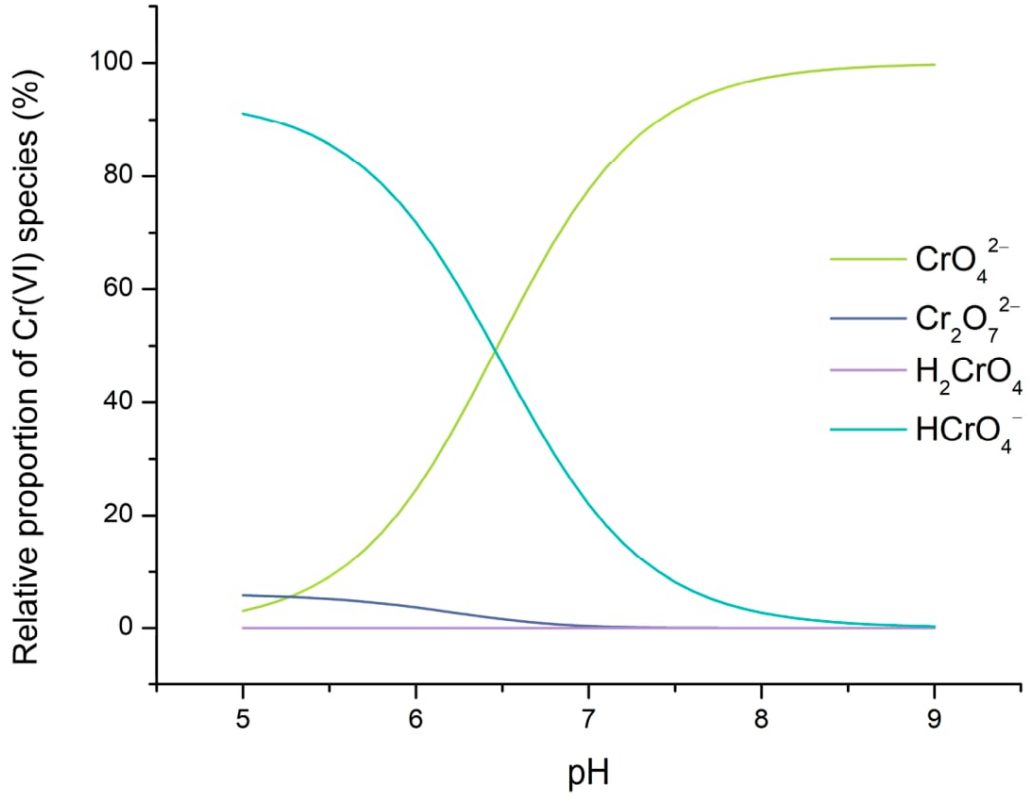


Figure 7. Calculated distribution of Cr(VI) species in the initial solution as a function of pH within the investigated range (pH 5–9), obtained using Visual MINTEQ 3.1 at an initial Cr(VI) concentration of 50 mg L^{-1}.

For MAC, the linear effect of solution pH was not statistically significant (F = 2.276, $p = 0.1573$), whereas the quadratic pH^2 term was significant (F = 16.646, $p = 0.0015$), indicating a nonlinear pH response (Table 3; Figure 8a–c). With the remaining factors fixed at their central levels and predictions averaged across the three experimental blocks, the fitted response increased from approximately 38.6% at pH 5 to a local maximum of approximately 52.4% near pH 6.7 and subsequently decreased to approximately 28.6% at pH 9. Thus, the fitted pH response was clearly non-monotonic. Among the interaction terms involving pH, the pH × dose interaction had a nominal *p*-value below 0.05 (F = 5.221, $p = 0.0413$; Figure 8b), whereas the pH × concentration interaction approached but did not reach this threshold (F = 4.492, $p = 0.0556$; Figure 8a).

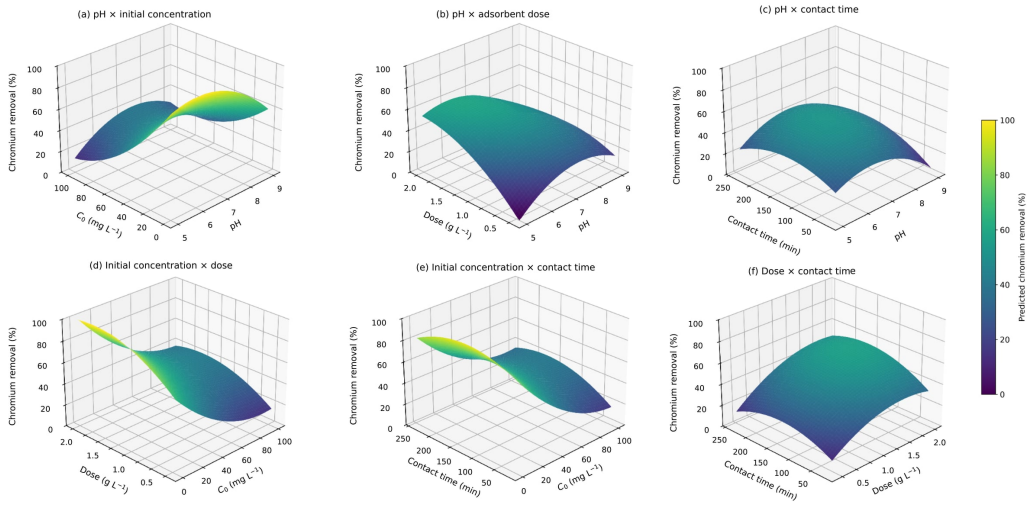


Figure 8. Three-dimensional response-surface plots showing the fitted effects of the investigated process variables on chromium removal by MAC: (**a**) pH × initial Cr(VI) concentration, (**b**) pH × adsorbent dose, (**c**) pH × contact time, (**d**) initial Cr(VI) concentration × adsorbent dose, (**e**) initial Cr(VI) concentration × contact time, and (**f**) adsorbent dose × contact time. For each panel, the two factors not displayed were held at their central levels (pH = 7, initial Cr(VI) concentration = 50.05 mg L^{-1}, adsorbent dose = 1.10 g L^{-1}, and contact time = 130 min, as applicable). Predictions were averaged across the three experimental blocks. A common 0–100% response scale was used for graphical presentation.

For MBC, neither the linear pH effect (F = 1.663, $p = 0.222$) nor the quadratic pH^2 term (F = 2.230, $p = 0.161$) was statistically significant (Table 4; Figure 9a–c). With the remaining factors fixed at their central levels and predictions averaged across the three experimental blocks, the fitted removal decreased only from approximately 14.0% at pH 5 to 10.4% at pH 9, consistent with the comparatively limited independent contribution of pH. However, the pH × contact-time interaction had a nominal *p*-value below 0.05 (F = 8.008, $p = 0.015$; Figure 9c), indicating that the fitted effect of contact time depended on pH. The magnitude of this interaction is examined quantitatively in Section 3.2.4.

The previously reported pHpzc values of 6.57 for MAC and 6.36 for MBC [20] provide useful physicochemical context for interpreting the pH response. Below the pHpzc, surface protonation is generally expected to increase the positive character of the adsorbent surface, whereas deprotonation becomes more pronounced above the pHpzc [34].

Such changes in surface charge may influence interactions with the predominantly anionic Cr(VI) species present within the investigated pH range, together with possible competition from OH^- ions [10,35]. However, the fitted MAC maximum near pH 6.7 occurs close to its pHpzc, where the net surface charge is expected to be relatively small. Therefore, the observed pH dependence cannot be explained by a simple monotonic electrostatic-

attraction mechanism alone. Although previous characterization confirmed the presence of carbonaceous and iron-containing phases in both materials [20], their specific contribution to chromium uptake was not directly determined in the present study. Accordingly, the calculated initial Cr(VI) speciation, surface-charge characteristics, and material composition are considered here as plausible physicochemical context rather than as experimentally demonstrated adsorption mechanisms.

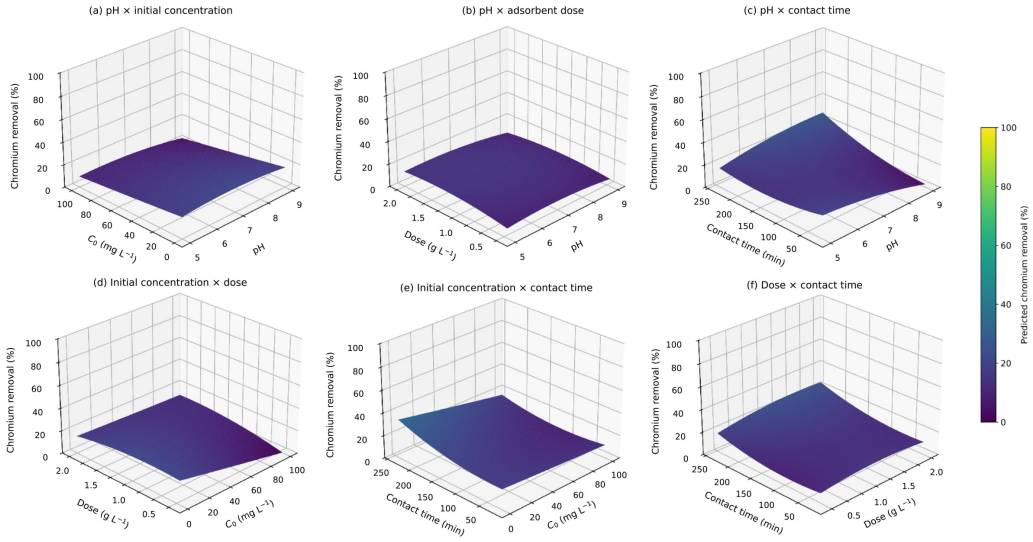


Figure 9. Three-dimensional response-surface plots showing the fitted effects of the investigated process variables on chromium removal by MBC: (**a**) pH × initial Cr(VI) concentration, (**b**) pH × adsorbent dose, (**c**) pH × contact time, (**d**) initial Cr(VI) concentration × adsorbent dose, (**e**) initial Cr(VI) concentration × contact time, and (**f**) adsorbent dose × contact time. For each panel, the two factors not displayed were held at their central levels (pH = 7, initial Cr(VI) concentration = 50.05 mg L^{-1}, adsorbent dose = 1.10 g L^{-1}, and contact time = 130 min, as applicable).

Overall, the effect of pH on chromium removal was adsorbent-dependent and cannot be described by a simple monotonic electrostatic relationship. For MAC, the fitted response was nonlinear, with a maximum near pH 6.7, close to the previously reported pHpzc, whereas for MBC the independent effect of pH was limited but became relevant through its interaction with contact time. These findings indicate that pH should be interpreted as part of a multivariable response rather than as evidence of a single adsorption mechanism.

3.2.2. Effect of Initial Cr(VI) Concentration

The initial Cr(VI) concentration is an important influent condition in adsorption systems, as it determines the amount of chromium available for interaction with the adsorbent [36].

For MAC, the initial Cr(VI) concentration was the most influential linear factor affecting chromium removal, with a highly significant effect observed by ANOVA ($F = 73.314$, $p < 0.0001$) (Table 3). The three-dimensional response surfaces consistently show decreasing predicted removal with increasing initial Cr(VI) concentration across its combinations with pH, adsorbent dose, and contact time (Figure 8a,d,e). With the remaining factors fixed at their central levels and predictions averaged across the three experimental blocks, increasing the initial Cr(VI) concentration from 0.10 to 100 mg L^{-1} decreased the fitted removal from approximately 96.2% to 39.3%. The significant concentration^2 term ($F = 11.876$, $p = 0.0048$) further indicates a nonlinear concentration response within the investigated range.

For MBC, initial Cr(VI) concentration also exhibited a statistically significant linear effect on chromium removal ($F = 17.317$, $p = 0.001$) (Table 4). The decreasing concentration response is visible across the corresponding surfaces with pH, adsorbent dose, and contact time (Figure 9a,d,e). With the remaining factors fixed at their central levels and predictions averaged across the three experimental blocks, increasing the initial concentration from 0.10 to 100 mg L^{-1} decreased the fitted removal from approximately 21.2% to 9.3%. In contrast to MAC, the quadratic concentration^2 term was not statistically significant ($F = 0.008$, $p = 0.932$), providing no evidence of pronounced curvature in the MBC concentration response.

The decrease in percentage removal with increasing initial Cr(VI) concentration is consistent with the general behaviour reported for adsorption systems in which the amount of solute increases relative to the available adsorbent surface and adsorption sites [37,38]. Although a higher initial concentration can increase the concentration gradient and thus the driving force for mass transfer, this does not necessarily translate into higher percentage removal [22]. The substantially larger fitted concentration effect observed for MAC than for MBC should be interpreted as a difference between the separately fitted response models rather than as evidence of a specific adsorption mechanism. Previously reported differences in the physicochemical properties of MAC and MBC [20] may provide contextual information, but their contribution to the different concentration responses was not directly tested in the present study.

3.2.3. Effect of Adsorbent Dose

Adsorbent dose was identified as a statistically significant factor affecting chromium removal by MAC ($F = 17.574$, $p = 0.0012$). The three-dimensional response surfaces show that the dose effect varied across its combinations with pH, initial Cr(VI) concentration, and contact time (Figure 8b,d,f). With the remaining factors fixed at their central levels and predictions averaged across the three experimental blocks, increasing the adsorbent dose from 0.20 to 2.00 g L^{-1} increased the fitted chromium removal from approximately 26.1% to 54.0%. The significant quadratic dose^2 term ($F = 7.044$, $p = 0.0210$) indicates that the dose response was nonlinear rather than proportional across the investigated range.

Similar nonlinear dose effects have been reported in adsorption systems and have been associated with phenomena such as particle aggregation and partial overlap of adsorption sites at higher adsorbent loadings. For magnetite-containing materials, magnetic interactions may additionally contribute to particle association [22]. However, particle aggregation, changes in particle size, and accessible surface area were not directly evaluated in the present study; therefore, these phenomena cannot be identified as the cause of the observed nonlinear dose response.

The pH × dose interaction had a nominal p-value below 0.05 ($F = 5.221$, $p = 0.0413$; Figure 8b), indicating that the fitted effect of adsorbent dose varied across the investigated pH range. Because the p-value was close to the 0.05 threshold, this interaction was interpreted cautiously. Similar pH-dependent dose effects have been reported in response-surface studies of Cr(VI) adsorption [10]; however, the underlying mechanism was not directly investigated in the present study.

For MBC, neither the linear dose term ($F = 1.123$, $p = 0.310$) nor the quadratic dose^2 term ($F = 2.680$, $p = 0.128$) was statistically significant (Table 4; Figure 9b,d,f). With the remaining factors fixed at their central levels and predictions averaged across the three experimental blocks, increasing the adsorbent dose from 0.20 to 2.00 g L^{-1} increased the fitted removal only from approximately 10.4% to 13.4%. Thus, the present data do not provide sufficient evidence for a clear independent dose effect within the investigated range.

Previously reported textural differences between MAC and MBC [20] provide useful physicochemical context for the different fitted dose–response patterns. However, these material properties were not included as explanatory variables in the present models, and their contribution to the observed statistical responses was not directly tested. They should therefore not be interpreted as establishing a causal mechanism for the different dose responses.

Overall, the fitted MAC model showed both linear and quadratic dose contributions together with a pH × dose interaction, whereas the corresponding dose terms in the MBC model did not reach the nominal $p = 0.05$ threshold. These results describe different within-model dose–response patterns; however, statistical significance in one separately fitted model and non-significance in the other does not constitute a formal test of a difference between the two adsorbents. No combined model including adsorbent × process-factor interaction terms was fitted; therefore, the present analysis does not provide a formal statistical test of differences in factor effects between MAC and MBC.

3.2.4. Effect of Contact Time

Contact time determines the duration of interaction between the initially Cr(VI)-containing solution and the adsorbent and may therefore influence the extent of chromium removal. In adsorption systems, time-dependent uptake may reflect several transport and surface processes [9,39]; however, the present design was not intended as a dedicated kinetic or diffusion experiment. Therefore, the fitted contact-time responses are interpreted here as statistical response patterns rather than as direct evidence of adsorption equilibrium or a specific rate-controlling mechanism.

For MAC, the linear contact-time term was not statistically significant ($F = 1.429$, $p = 0.255$), whereas the quadratic contact-time^2 term was significant ($F = 8.091$, $p = 0.0148$), indicating a nonlinear response (Table 3; Figure 8c,e,f). With the remaining factors fixed at their central levels and predictions averaged across the three experimental blocks, the fitted removal increased from approximately 35.2% at 20 min to a local maximum of approximately 52.4% at about 147 min and subsequently decreased to approximately 43.2% at 240 min. Thus, the fitted response describes a local maximum rather than a plateau, and it should not be interpreted as evidence that adsorption equilibrium was reached.

For MBC, both the linear contact-time term ($F = 14.495$, $p = 0.002$) and the quadratic contact-time^2 term ($F = 6.127$, $p = 0.029$) were statistically significant (Table 4; Figure 9c,e,f). In contrast to MAC, both fitted coefficients were positive. At the central levels of the remaining factors and with predictions averaged across the three experimental blocks, increasing contact time from 20 to 240 min increased the fitted removal from approximately 14.5% to 25.3%. The positive quadratic coefficient indicates upward curvature rather than a progressively diminishing response at longer contact times.

The pH × contact-time interaction in the MBC model was statistically significant ($F = 8.008$, $p = 0.015$; Figure 9c), indicating that the fitted effect of contact time depended on solution pH. With initial Cr(VI) concentration and adsorbent dose fixed at their central levels and predictions averaged across the three experimental blocks, increasing contact time from 20 to 240 min changed the fitted removal from approximately 20.4% to 17.3% at pH 5, from 14.5% to 25.3% at pH 7, and from 2.8% to 27.5% at pH 9. These contrasts demonstrate that the contact-time response in the fitted MBC model varied substantially across the investigated pH range.

Previously reported textural differences between MAC and MBC [20], including differences in specific surface area, micropore volume, and average pore size, provide useful physicochemical context for the different fitted contact-time patterns. However, no dedicated kinetic model, diffusion analysis, or particle-size-dependent transport study was

performed in the present work. Accordingly, the observed responses cannot be attributed specifically to external mass transfer, intraparticle diffusion, pore-size effects, or progressive site saturation.

Previous studies of magnetic carbonaceous adsorbents have reported time-dependent Cr(VI) removal involving multiple surface and transport processes [40]. Such mechanisms may provide useful literature context, but they were not directly demonstrated for the present MAC and MBC systems. No Cr(III) or other oxidation-state measurements were performed; therefore, Cr(VI) reduction cannot be established from the present data.

Overall, the separately fitted response-surface models showed different contact-time patterns for the two adsorbents. MAC exhibited a quadratic response with a fitted local maximum at approximately 147 min, whereas MBC showed positive linear and quadratic contact-time contributions together with a significant pH × contact-time interaction. These differences describe the behaviour of the separately fitted models and should not be interpreted as formal evidence of different kinetic mechanisms between MAC and MBC.

3.2.5. Response-Metric Sensitivity Based on Chromium Uptake

To assess whether the observed response patterns were sensitive to the choice of performance metric, chromium uptake q_t was additionally evaluated for all experimental runs. The corresponding lnq_t models showed that initial Cr(VI) concentration remained the dominant term for both materials (MAC: $F = 164.37$, $p < 0.0001$; MBC: $F = 1713.16$, $p < 0.0001$), although the relative contributions of the other process variables differed from those obtained using removal efficiency. For MAC, the quadratic concentration and contact-time terms were also significant, whereas the linear dose term did not reach the nominal significance threshold ($p = 0.103$). For MBC, significant contributions were observed for adsorbent dose, contact time, pH, and several quadratic and interaction terms (Table S3). Experimental and RSM-fitted chromium uptake values for all runs are provided in Table S2.

This complementary analysis highlights that removal efficiency and chromium uptake emphasize different aspects of adsorption performance. For example, for MAC, 96.16% removal at an initial Cr(VI) concentration of 0.10 mg L^{-1} corresponded to a chromium uptake of only 0.087 mg g^{-1}, whereas 53.94% removal at 50.05 mg L^{-1} corresponded to 24.54 mg g^{-1}. Thus, high percentage removal at low initial concentration does not necessarily correspond to high chromium uptake per unit mass of adsorbent, and the apparent relative importance of the investigated factors partly depends on the response metric considered. At the same time, the uptake-based results should be interpreted within the structure of the Box–Behnken design, in which initial concentration, pH, adsorbent dose, and contact time were varied simultaneously. Consequently, the calculated q_t values represent chromium uptake at the specific contact time and experimental conditions of each run and should not be interpreted as equilibrium adsorption capacities or maximum capacities q_{max}. A dedicated equilibrium-isotherm study under constant experimental conditions would be required for rigorous determination of equilibrium parameters and maximum adsorption capacity.

3.3. Model Validation and Optimization of Process Parameters

The second-order polynomial regression equations developed using RSM are presented below. These equations describe the fitted relationship between the investigated operating variables and chromium removal efficiency within the experimental design space. The regression coefficients represent the linear, quadratic, and interaction effects of the independent variables on the fitted response. Equations (7) and (8) are expressed in coded factor units. The continuous variables were centred and scaled according to the factor levels defined in Table 1, with −1, 0, and +1 corresponding to the lower, central, and upper levels,

respectively. The block terms are represented by indicator variables, with Block 1 used as the reference category.

$$\begin{aligned}\text{Chromium Removal (MAC)} = {} & +47.2970\ (\text{Intercept}) + 3.8470\ (\text{Block 2}) + \\ & 10.5697\ (\text{Block 3}) - 5.0179\ \text{pH} - 28.4786\ \text{Concentration} + 13.9431\ \text{Dose} + \\ & 3.9762\ \text{Contact_time} - 18.5005\ \text{I}(\text{pH}^2) + 15.6265\ \text{I}(\text{Concentration}^2) - \\ & 12.0346\ \text{I}(\text{Dose}^2) - 12.8978\ \text{I}(\text{Contact_time}^2) + 12.2093\ \text{pH:Concentration} - \\ & 13.1634\ \text{pH:Dose} + 5.4445\ \text{pH:Contact_time} - 3.1714\ \text{Concentration:Dose} + \\ & 4.9959\ \text{Concentration:Contact_time} + 3.2789\ \text{Dose:Contact_time}\end{aligned} \quad (7)$$

$$\begin{aligned}\text{Chromium Removal (MBC)} = {} & +14.2270\ (\text{Intercept}) - 1.0015\ (\text{Block 2}) + \\ & 3.5659\ (\text{Block 3}) - 1.8331\ \text{pH} - 5.9155\ \text{Concentration} + 1.5063\ \text{Dose} + \\ & 5.4122\ \text{Contact_time} - 2.8938\ \text{I}(\text{pH}^2) + 0.1683\ \text{I}(\text{Concentration}^2) - \\ & 3.1729\ \text{I}(\text{Dose}^2) + 4.7973\ \text{I}(\text{Contact_time}^2) - 1.3674\ \text{pH:Concentration} - \\ & 0.9786\ \text{pH:Dose} + 6.9678\ \text{pH:Contact_time} + 4.2598\ \text{Concentration:Dose} - 2.9645 \\ & \text{Concentration:Contact_time} + 1.4992\ \text{Dose:Contact_time}\end{aligned} \quad (8)$$

Positive regression coefficients indicate that an increase in the corresponding coded variable tends to increase the predicted response, whereas negative coefficients indicate the opposite effect. Because the continuous factors were expressed in coded units, the coefficient magnitudes provide an indication of the direction and strength of the fitted effects, while their statistical significance is evaluated by ANOVA (Section 3.1).

Based on the fitted quadratic response-surface models, numerical optimization was performed to identify the conditions associated with maximum predicted chromium removal within the nominal factor bounds. Accordingly, the reported solution represents a removal-efficiency-based model prediction and should not be interpreted as the condition that maximizes chromium uptake (q_t). For MAC, the model-predicted conditions associated with maximum removal were pH 5.33, an initial Cr(VI) concentration of 0.10 mg L^{-1}, an adsorbent dose of 2.00 g L^{-1} and a contact time of 120.3 min. Under these conditions, the unconstrained quadratic model returned a removal efficiency of 109.1%. Because removal efficiency cannot physically exceed 100%, this value represents mathematical overshoot of the polynomial response surface rather than a physically achievable prediction. Therefore, values above 100% were not interpreted quantitatively; instead, the optimization result was taken to indicate a region associated with very high predicted chromium removal.

The predicted MAC solution should nevertheless be interpreted cautiously. Although all factor values remained within their nominal experimental ranges, the solution occurred at the minimum initial Cr(VI) concentration and maximum adsorbent dose and was located outside the region directly sampled by the Box–Behnken design. Thus, the prediction involves response-surface extrapolation within the nominal factor bounds. In addition, initial Cr(VI) concentration represents an influent condition rather than a controllable treatment variable; consequently, the value of 0.10 mg L^{-1} should not be interpreted as an operational optimum.

The blocks were included as additive categorical terms without interactions with the process factors, so block membership did not change the location of the predicted maximum but did affect the predicted response level. For MAC, relative to the Block 1 prediction reported above, the same factor settings yielded approximately 113% and 120% for Blocks 2 and 3, respectively. For MBC, the corresponding predictions were approximately 37.5%, 36.5%, and 41.1% for Blocks 1, 2, and 3, respectively. These differences reflect the additive block coefficients and further support interpreting the optimization results as model-based predictions rather than uniquely defined physical optima.

Moreover, maximizing percentage removal at very low influent concentration and high adsorbent dose does not necessarily correspond to the most resource-efficient treatment condition. This is consistent with the uptake-based sensitivity analysis in Section 3.2.5, which showed that high percentage removal at low initial concentration can correspond to substantially lower chromium uptake per unit mass of adsorbent. In addition, at an influent concentration of 0.10 mg L^{-1}, a 50% reduction would already decrease the concentration to 0.05 mg L^{-1}, corresponding to the guideline value cited in the Introduction. Thus, the model-predicted maximum of removal efficiency should not be interpreted as the most practically efficient treatment condition.

For MBC, numerical optimization identified the highest predicted chromium removal within the nominal factor bounds at pH 9.00, an initial Cr(VI) concentration of 0.10 mg L^{-1}, an adsorbent dose of 0.783 g L^{-1}, and a contact time of 240 min, corresponding to a predicted removal efficiency of 37.49% for the reference block. It occurred at the upper boundaries of the investigated pH and contact-time ranges and, like the MAC solution, outside the region directly sampled by the Box–Behnken design. Furthermore, neither the linear nor the quadratic effect of pH was statistically significant in the developed RSM model; therefore, pH 9 should not be interpreted as evidence that alkaline conditions are inherently optimal for chromium removal by MBC.

The fitted RSM models provided useful descriptions of the response surfaces within the investigated experimental domain; however, the optimization results should be interpreted as model-based predictions rather than independently validated optimum operating conditions. Although the three-level Box–Behnken design was sufficient to estimate the full quadratic models, it does not guarantee uniform predictive reliability throughout the entire factor space. The moderate LOOCV performance for MAC and the weaker goodness-of-fit and limited cross-validated performance for MBC further support cautious interpretation of the predicted optimum regions. Future studies could augment the present design with additional boundary or axial points, for example through a Central Composite Design, to improve resolution of these regions and enable more robust experimental validation.

3.4. Comparison of RSM and Machine-Learning Models

Machine-learning models were developed as a complementary approach to RSM to evaluate predictive capability and assess the relative importance of the investigated process variables. Random Forest (RF) and Support Vector Regression (SVR) were implemented as exploratory data-driven models using the same experimental dataset as the RSM model. To enable a consistent comparison of predictive performance, all models were evaluated using leave-one-out cross-validation (LOOCV), which is particularly suitable for small experimental datasets because each observation is used once for validation while the remaining observations are used for model training. Model performance was evaluated using the coefficient of determination (R^2), root mean square error (RMSE), and mean absolute error (MAE). For SVR, feature standardization was performed within the cross-validation pipeline to avoid information leakage between the training and validation data.

The LOOCV results for the MAC dataset are summarized in Table 5. Random Forest yielded the numerically highest cross-validated performance (R^2 = 0.613; RMSE = 17.359; MAE = 13.635), whereas SVR yielded R^2 = 0.456, RMSE = 20.586, and MAE = 15.671. The RSM model yielded a LOOCV R^2 of 0.459, with RMSE and MAE values of 20.529 and 17.530, respectively.

Table 5. LOOCV performance of RSM and machine-learning models for the MAC.

Model	Validation Method	R^2	RMSE	MAE
RSM	LOOCV	0.459	20.53	17.53
Random Forest	LOOCV	0.613	17.36	13.64
Support Vector Regression	LOOCV	0.456	20.59	15.67

A similar machine-learning analysis was performed for the MBC dataset and is provided in the Supplementary Information (Table S4). Under the same LOOCV framework, all models showed substantially lower predictive performance for MBC than for MAC, with cross-validated R^2 values ranging from −0.044 to 0.168. Notably, the RSM model for MBC yielded a LOOCV R^2 of −0.044, indicating that, under this validation framework, its out-of-sample predictions did not outperform a mean-response baseline. Inclusion of experimental block as a categorical predictor did not produce a consistent improvement in predictive performance: the RF R^2 decreased from 0.168 to 0.087, whereas the SVR R^2 changed only marginally from 0.166 to 0.182. Bootstrap uncertainty analysis further showed that the 95% confidence intervals for all pairwise model differences in R^2, RMSE, and MAE included zero, providing no evidence for a clear ranking among the evaluated models. Additional block-aware and bootstrap uncertainty analyses for the MBC models are provided in Table S5 and did not alter the overall conclusion that cross-validated predictive performance remained limited and that no clear ranking among the evaluated models was supported. Ultimately, the suppressed predictive performance of the MBC models may be attributable to constrained response variability within the dataset, although this explanation remains speculative rather than conclusively established. During the experimental design phase, uniform experimental conditions were intentionally maintained for both the MAC and MBC adsorbents to facilitate a direct comparison. However, as illustrated by their respective response surfaces (Figures 8 and 9), these shared operational parameters may have been less suitable for capturing the response behaviour of the MBC system, which exhibited a relatively narrow range of chromium removal efficiencies (0–38%), in contrast to the full range of 0–100% observed for MAC. It is therefore plausible that this restricted response range contributed to the lower predictive performance of the MBC models, although other factors may also have played a role. Adjusting the initial Cr(VI) concentration downward or increasing the MBC adsorbent dosage might have produced a wider range of removal efficiencies and potentially improved model performance. However, these adjustments would have compromised the systematic comparability of the two adsorbents under the same experimental conditions.

Therefore, the detailed comparison between RSM and machine-learning approaches presented here focuses on the MAC dataset, for which the models showed stronger cross-validated predictive performance and provided a more informative basis for comparing the modelling approaches.

Because the RSM models included experimental block as a categorical nuisance term, an additional sensitivity analysis was performed in which block membership was also included as a categorical predictor in the RF and SVR models. Inclusion of block did not improve cross-validated predictive performance. For RF, the LOOCV R^2 decreased from 0.613 to 0.578 (RMSE: 17. 9 to 18.134; MAE: 13.635 to 14.886), while for SVR it decreased from 0.456 to 0.396 (RMSE: 20.586 to 21.689; MAE: 15.671 to 17.351). These results indicate that explicit inclusion of block did not provide additional predictive information for the machine-learning models within the present dataset. Accordingly, the primary ML comparison was retained using the four experimental input variables, while the block-aware results were considered as a sensitivity analysis.

The cross-validation results provide a different perspective from the goodness-of-fit statistics obtained for the final RSM model. Although the quadratic RSM model provided a strong fit to the complete MAC dataset ($R^2 = 0.929$), its LOOCV performance was lower ($R^2 = 0.459$). This difference indicates that the high goodness of fit of the RSM model should not be interpreted as equivalent to out-of-sample predictive performance. Random Forest yielded numerically better cross-validated performance than the other evaluated approaches ($R^2 = 0.613$), although substantial unexplained variability remained.

Uncertainty analysis based on 10,000 paired bootstrap resamples further showed that the apparent differences in cross-validated performance should be interpreted cautiously. For RF versus RSM, the difference in R^2 was 0.172 (95% CI: −0.094 to 0.481), while the difference in RMSE was −3.287 percentage points (95% CI: −7.769 to 1.576); both intervals included zero. The RF–RSM difference in MAE was −3.910 percentage points (95% CI: −7.143 to −0.610), indicating lower absolute prediction error for RF under this resampling analysis. Pairwise comparisons between RF and SVR and between RSM and SVR produced confidence intervals that included zero for all three metrics. Thus, although RF yielded numerically better overall LOOCV performance, the uncertainty analysis does not support a definitive ranking of the evaluated models based on R^2 and RMSE.

The reduction in predictive performance under cross-validation is not unexpected given the small experimental dataset ($n = 29$). Because the Box–Behnken design contains structured and partly unique design points, leaving out a single run can require prediction at a design location that is not represented identically in the remaining training data. Accordingly, LOOCV in this setting should be interpreted partly as an extrapolation stress test rather than as a pure interpolation assessment. This characteristic may affect model classes differently and limits strong ranking claims based on small differences in LOOCV performance. The cross-validation results should therefore be interpreted as a comparative assessment within the present experimental design rather than as definitive evidence of model superiority.

Accordingly, RSM and machine learning provided complementary information in the present study. RSM enabled direct statistical evaluation of linear, quadratic, and interaction effects and supported model-based numerical optimization, whereas Random Forest provided an alternative data-driven assessment of predictive performance and variable importance. Given the limited dataset size, the machine-learning results should be interpreted as exploratory and complementary rather than as evidence of broadly generalizable predictive models.

To further investigate the relative importance of the investigated process variables, a detailed Random Forest feature-importance analysis was performed for the MAC dataset. The resulting variable ranking is presented in Table 6.

Table 6. Random Forest feature-importance stability for the MAC dataset.

Variable	Mean Importance (%)	SD (%)	Mean Rank	Rank 1 Frequency (%)
Initial Cr(VI) concentration	59.36	0.97	1.00	100
pH	16.12	0.76	2.27	0
Adsorbent dose	15.51	0.52	2.73	0
Contact time	9.01	0.49	4.00	0

Note: Feature importance was quantified using the impurity-based Random Forest measure (mean decrease in impurity). Values represent the mean and standard deviation across 30 Random Forest fits using 200 trees per model and different random seeds.

The repeated Random Forest analysis showed a stable feature-importance ranking for MAC (Table 6). Initial Cr(VI) concentration received the highest mean impurity-based importance (59.36 ± 0.97%) and was ranked first in all 30 repeated fits. Mean importance values for pH, adsorbent dose, and contact time were 16.12 ± 0.76%, 15.51 ± 0.52%, and 9.01 ± 0.49%, respectively. These values describe the relative contribution of the input variables to the fitted Random Forest model and should not be interpreted as measures of statistical significance or causal influence on chromium adsorption.

Qualitatively, the high Random Forest importance assigned to initial Cr(VI) concentration is consistent with its prominent contribution to the fitted RSM response. However, Random Forest feature importance and ANOVA statistics quantify different aspects of variable influence and were therefore not compared numerically. Taken together, the RSM and machine-learning analyses provide complementary but methodologically distinct perspectives on the experimental response, and their interpretation should remain within the limits of the present dataset and study design.

The present study was designed primarily to evaluate factor effects, response-surface behaviour, and model-based optimization under controlled batch conditions. Practical application of the materials for treatment of Cr(VI)-containing waters was not directly evaluated. In particular, regeneration and reuse, competing ions, natural organic matter, real-water matrices, iron leaching, treatment cost, and scale-up were outside the scope of the present experiments. Although the same MAC and MBC materials have previously been evaluated under more application-oriented conditions for arsenic removal [20], those findings cannot be directly transferred to the present chromium system. Therefore, practical implementation of these materials for chromium removal from Cr(VI)-containing waters will require dedicated validation under realistic water matrices and repeated-use conditions.

4. Conclusions

Response Surface Methodology using a Box–Behnken design was applied to investigate chromium removal from initially Cr(VI)-containing solutions using MAC and MBC and to perform model-based numerical optimization within the investigated experimental domain. The developed quadratic models revealed distinct response patterns for the two magnetic carbon nanocomposites and differences in the relative contributions of the investigated process variables.

The quadratic RSM model provided a strong fit to the experimental data for MAC ($R^2 = 0.929$, adjusted $R^2 = 0.835$), whereas the MBC model was also statistically significant but exhibited a weaker fit ($R^2 = 0.846$, adjusted $R^2 = 0.640$). Numerical optimization identified model-predicted high-removal conditions for MAC; however, the unconstrained quadratic model produced a value above the physical 100% limit, which was interpreted as mathematical overshoot rather than as an achievable removal efficiency. The model-predicted optimum for MBC occurred at the boundary of the experimental domain and was therefore interpreted cautiously. Under a common LOOCV framework, Random Forest yielded the numerically highest predictive performance for MAC ($R^2 = 0.613$), compared with RSM ($R^2 = 0.459$) and SVR ($R^2 = 0.456$). However, bootstrap uncertainty analysis showed that the observed differences did not support a definitive overall ranking of the evaluated models. For MBC, all evaluated models showed limited cross-validated predictive performance, and no clear ranking was supported. These findings emphasize the distinction between goodness-of-fit within a structured response-surface design and prediction of observations excluded from model development.

Random Forest feature-importance analysis assigned the highest importance to initial Cr(VI) concentration for MAC, consistent with its strong contribution in the ANOVA analysis. Differences observed for the remaining variables illustrate that statistical significance

and machine-learning feature importance represent different aspects of variable influence. In this context, RSM and machine learning should be regarded as complementary rather than competing approaches: RSM provides direct interpretation of linear, quadratic, and interaction effects and supports model-based numerical optimization within the investigated design space, whereas machine-learning methods provide additional information on cross-validated predictive performance and variable importance.

The present findings should be interpreted within the scope of the controlled batch experiments performed in this study. Regeneration and reuse, competing ions, natural organic matter, real-water matrices, iron leaching, treatment cost, and scale-up were not directly evaluated for chromium removal from Cr(VI)-containing solutions. Although the same MAC and MBC materials were previously investigated under more application-oriented conditions for arsenic removal [20], those findings cannot be directly transferred to the present chromium system.

Future studies should therefore address these limitations through dedicated equilibrium-isotherm experiments under controlled conditions, repeated-use studies, and validation in realistic water matrices containing competing ions and natural organic matter. Such equilibrium studies would enable rigorous determination of adsorption parameters and maximum adsorption capacity, as well as systematic comparison of MAC and MBC with other Cr(VI) adsorbents reported in the literature under comparable experimental conditions. Additional characterization and regeneration studies would further support mechanistic interpretation and assessment of practical applicability, while larger and more diverse datasets would allow a more rigorous evaluation of the additional predictive value of machine-learning approaches beyond conventional response-surface models.

Overall, the combined use of structured experimental design, response-surface modelling, and complementary machine-learning analysis provides a useful framework for investigating adsorption processes and may support future data-driven development and optimization of magnetic adsorbents for water treatment.

Supplementary Materials: The following supporting information can be downloaded at: https://www.mdpi.com/article/10.3390/pr14213497/s1. Table S1. Experimental conditions and corresponding experimental and predicted chromium removal efficiencies for MAC and MBC. Table S2. Experimental and RSM-fitted chromium uptake qt values for MAC and MBC. Table S3. Sensitivity analysis of ln(qt) using the full quadratic RSM models. Table S4. LOOCV performance of RSM and machine-learning models for the MBC dataset. Table S5. Block-aware sensitivity and bootstrap uncertainty analysis for the MBC dataset.

Author Contributions: J.N.: Investigation, conceptualization, formal analysis, software, visualization; writing—original draft preparation, writing—review and editing; M.Š.: investigation, formal analysis, visualization; writing—original draft preparation; A.K.M.: investigation, formal analysis, visualization, writing—original draft preparation; J.P.B.: investigation, visualization, writing—original draft preparation; M.B.K.: investigation, formal analysis, writing—original draft preparation; M.W.: formal analysis, writing—original draft preparation; writing—review and editing; J.A.: formal analysis, writing—review and editing, funding acquisition. All authors have read and agreed to the published version of the manuscript.

Funding: This work was supported by the Ministry of Science, Technological Development and Innovation of the Republic of Serbia (Grants No. 451-03-33/2026-03/200125 & 451-03-34/2026-03/200125).

Data Availability Statement: The data supporting the findings of this study are available within the article and its Supplementary Materials. Additional data are available from the corresponding author upon reasonable request.

Conflicts of Interest: The authors declare no conflicts of interest.

Abbreviations

The following abbreviations are used in this manuscript:

MAC	Magnetic activated carbon
MBC	Magnetic biochar
RSM	Response Surface Methodology
ANOVA	Analysis of variance
WHO	World Health Organization
R^2	Coefficient of determination
RMSE	Root mean square error
MAE	Mean absolute error
ANN	Artificial Neural Networks
RF	Random Forest
SVR	Support Vector Regression

References

1. Tumolo, M.; Ancona, V.; De Paola, D.; Losacco, D.; Campanale, C.; Massarelli, C.; Uricchio, V.F. Chromium Pollution in European Water, Sources, Health Risk, and Remediation Strategies: An Overview. *Int. J. Environ. Res. Public Health* **2020**, *17*, 5438. [CrossRef] [PubMed]
2. Irshad, M.A.; Sattar, S.; Nawaz, R.; Al-Hussain, S.A.; Rizwan, M.; Bukhari, A.; Waseem, M.; Irfan, A.; Inam, A.; Zaki, M.E.A. Enhancing Chromium Removal and Recovery from Industrial Wastewater Using Sustainable and Efficient Nanomaterial: A Review. *Ecotoxicol. Environ. Saf.* **2023**, *263*, 115231. [CrossRef] [PubMed]
3. Wu, Z.; Zhang, H.; Ali, E.; Shahab, A.; Huang, H.; Ullah, H.; Zeng, H. Synthesis of Novel Magnetic Activated Carbon for Effective Cr(VI) Removal via Synergistic Adsorption and Chemical Reduction. *Environ. Technol. Innov.* **2023**, *30*, 103092. [CrossRef]
4. Prasad, S.; Yadav, K.K.; Kumar, S.; Gupta, N.; Cabral-Pinto, M.M.S.; Rezania, S.; Radwan, N.; Alam, J. Chromium Contamination and Effect on Environmental Health and Its Remediation: A Sustainable Approaches. *J. Environ. Manag.* **2021**, *285*, 112174. [CrossRef] [PubMed]
5. Iyer, M.; Anand, U.; Thiruvenkataswamy, S.; Babu, H.W.S.; Narayanasamy, A.; Prajapati, V.K.; Tiwari, C.K.; Gopalakrishnan, A.V.; Bontempi, E.; Sonne, C.; et al. A Review of Chromium (Cr) Epigenetic Toxicity and Health Hazards. *Sci. Total Environ.* **2023**, *882*, 163483. [CrossRef] [PubMed]
6. Alvarez, C.C.; Bravo Gómez, M.E.; Hernández Zavala, A. Hexavalent Chromium: Regulation and Health Effects. *J. Trace Elem. Med. Biol.* **2021**, *65*, 126729. [CrossRef] [PubMed]
7. Liang, C.; Wu, H.; Chen, J.; Wei, Y. Mechanistic Insights into the Interfacial Adsorption Behaviors of Cr(VI) on Ferrihydrite: Effects of PH and Naturally Coexisting Anions in the Environment. *Ecotoxicol. Environ. Saf.* **2023**, *249*, 114474. [CrossRef] [PubMed]
8. Xie, S. Water Contamination Due to Hexavalent Chromium and Its Health Impacts: Exploring Green Technology for Cr (VI) Remediation. *Green Chem. Lett. Rev.* **2024**, *17*, 2356614. [CrossRef]
9. Afshin, S.; Rashtbari, Y.; Vosough, M.; Dargahi, A.; Fazlzadeh, M.; Behzad, A.; Yousefi, M. Application of Box–Behnken Design for Optimizing Parameters of Hexavalent Chromium Removal from Aqueous Solutions Using Fe_3O_4 Loaded on Activated Carbon Prepared from Alga: Kinetics and Equilibrium Study. *J. Water Process Eng.* **2021**, *42*, 102113. [CrossRef]
10. Yao, W.; Tai, D.; Zeng, H.; Zhang, H.; Huang, H. Magnetic Activated Carbon Optimization Using Response Surface Approach for Cr(VI). *IOP Conf. Ser. Earth Environ. Sci.* **2022**, *1087*, 012002. [CrossRef]
11. Tabana, L.; Kupa, A.; Tichapondwa, S. Adsorption of Hexavalent Chromium from Wastewater Using Magnetic Biochar Derived from Peanut Hulls. *Phys. Chem. Earth* **2025**, *137*, 103815. [CrossRef]
12. World Health Organization. *Guidelines for Drinking-Water Quality: Fourth Edition Incorporating the First and Second Addenda*; World Health Organization: Geneva, Switzerland, 2022; ISBN 978-92-4-004506-4.
13. Assefa, H.; Singh, S.; Olu, F.E.; Dhanjal, D.S.; Mani, D.; Khan, N.A.; Singh, J.; Ramamurthy, P.C. Advances in Adsorption Technologies for Hexavalent Chromium Removal: Mechanisms, Materials, and Optimization Strategies. *Desalin. Water Treat.* **2024**, *319*, 100576. [CrossRef]
14. Malouchi, N.; Bakola, V.; Kotrotsiou, O.; Plakas, K.V.; Kostoglou, M.; Katsoyiannis, I.A. Critical Review of Cr (VI) Removal Technologies from Water and Wastewater. *Sustainability* **2026**, *18*, 6646. [CrossRef]
15. Kumari, A.; Kamaraj, N.; Selvaraj, R.; Nanoth, R. Emerging Trends and Future Outlook on Chromium Removal in the Lab, Pilot Scale, and Industrial Wastewater System: An Updated Review Exploring 10 Years of Research. *Environ. Monit. Assess.* **2025**, *197*, 547. [CrossRef] [PubMed]

16. Liu, B.; Xin, Y.N.; Zou, J.; Khoso, F.M.; Liu, Y.P.; Jiang, X.Y.; Peng, S.; Yu, J.G. Removal of Chromium Species by Adsorption: Fundamental Principles, Newly Developed Adsorbents and Future Perspectives. *Molecules* **2023**, *28*, 639. [CrossRef] [PubMed]
17. Zeng, W.; Luo, Y.; Wang, C.; Liu, Z.; Xue, M.; Xie, X. A Review on Recent Advances of Adsorption and Photoreduction of Cr(VI). *Environ. Pollut. Bioavailab.* **2025**, *37*, 2493057. [CrossRef]
18. Juturu, R.; Selvaraj, R.; Murty, V.R. Efficient Removal of Hexavalent Chromium from Wastewater Using a Novel Magnetic Biochar Composite Adsorbent. *J. Water Process Eng.* **2024**, *66*, 105908. [CrossRef]
19. Nikić, J.; Watson, M.; Tubić, A.; Šolić, M.; Agbaba, J. Recent Trends in the Application of Magnetic Nanocomposites for Heavy Metals Removal from Water: A Review. *Sep. Sci. Technol.* **2024**, *59*, 293–331. [CrossRef]
20. Šolić, M.; Pešić Bajić, J.; Govedarica, J.J.; Apostolović, T.; Koljaja, M.B.; Nikić, J. Magnetic Carbon-Based Nanocomposites for Arsenic Removal: Comparative Performance, Mechanistic Insights and Continuous-Flow Validation. *Surf. Interfaces* **2026**, *97*, 110011. [CrossRef]
21. Kang, K.; Hu, Y.; Khan, I.; He, S.; Fetahi, P. Recent Advances in the Synthesis and Application of Magnetic Biochar for Wastewater Treatment. *Bioresour. Technol.* **2023**, *390*, 129786. [CrossRef] [PubMed]
22. Mungwari, C.P.; Chetse, M.; Sigauke, P.; Chigondo, F.; Shumba, M.; Matshitse, R.; Nyamunda, B.C. Application of RSM and ANN Modelling Techniques in the Removal of Cr (VI) from Aqueous Solution Using PANI@ Fe_3O_4@green Moringa Leaves Biomass, a Hybrid Magnetic Nanocomposite. *Next Nanotechnol.* **2026**, *9*, 100456. [CrossRef]
23. Shakoor, M.B.; Khalil, U.; Ali, S.; Sharif, F.; Ahmad, S.R.; Rizwan, M.; Jilani, A.; Al-Ghanim, K.A.; Sarker, P.K. Microwave-Assisted Magnetic Biochar for Removal of Hexavalent Chromium from Aqueous Solution. *Environ. Pollut. Bioavailab.* **2024**, *36*, 2368590. [CrossRef]
24. Montgomery, D.C. *Design and Analysis of Experiments*, 9th ed.; Wiley: Hoboken, NJ, USA, 2017; ISBN 9781119113478.
25. Myers, R.H.; Montgomery, D.C.; Anderson-Cook, C.M. *Response Surface Methodology: Process and Product Optimization Using Designed Experiments*, 4th ed.; John Wiley & Sons: Hoboken, NJ, USA, 2016.
26. Khorsheed, A.; Asadi, K.; Asadi, F.; Aydoğmuş, R.; Erzen, E.; Karataş, B.; Deniz, M.; Orhan, Ş. Process Optimization with Response Surface Methodology: A Comprehensive Approach by Experimental Design Types. *Int. J. Adv. Nat. Sci. Eng. Res. (IJANSER)* **2025**, *12*, 546–558.
27. Bezerra, M.A.; Santelli, R.E.; Oliveira, E.P.; Villar, L.S.; Escaleira, L.A. Response Surface Methodology (RSM) as a Tool for Optimization in Analytical Chemistry. *Talanta* **2008**, *76*, 965–977. [CrossRef] [PubMed]
28. Ferreira, S.L.C.; Bruns, R.E.; Ferreira, H.S.; Matos, G.D.; David, J.M.; Brandão, G.C.; da Silva, E.G.P.; Portugal, L.A.; dos Reis, P.S.; Souza, A.S.; et al. Box-Behnken Design: An Alternative for the Optimization of Analytical Methods. *Anal. Chim. Acta* **2007**, *597*, 179–186. [CrossRef] [PubMed]
29. Javid, A.; Roudbari, A.; Yousefi, N.; Fard, M.A.; Barkdoll, B.; Talebi, S.S.; Nazemi, S.; Ghanbarian, M.; Ghadiri, S.K. Modeling of chromium (VI) removal from aqueous solution using modified green-Graphene: RSM-CCD approach, optimization, isotherm, and kinetic studies. *J. Environ. Health Sci. Eng.* **2020**, *18*, 515–529. [CrossRef] [PubMed]
30. Zhigalenok, Y.; Tazhibayeva, A.; Kokhmetova, S.; Starodubtseva, A.; Kan, T.; Isbergenova, D.; Malchik, F. Hexavalent chromium at the crossroads of science, environment and public health. *RSC Adv.* **2025**, *15*, 21439–21464. [CrossRef] [PubMed]
31. U.S. Environmental Protection Agency. *Method 6020B (SW-846)*; Inductively Coupled Plasma-Mass Spectrometry. Revision 2; EPA: Washington, DC, USA, 2014.
32. Zewde, Z.; Asere, T.G.; Yitbarek, M. Porous Biochars Derived from Brewery Waste for the Treatment of Cr(VI)-Contaminated Water. *PLoS ONE* **2024**, *19*, e0314522. [CrossRef] [PubMed]
33. Sinha, R.; Kumar, R.; Abhishek, K.; Shang, J.; Bhattacharya, S.; Sengupta, S.; Kumar, N.; Singh, R.K.; Mallick, J.; Kar, M.; et al. Single-Step Synthesis of Activated Magnetic Biochar Derived from Rice Husk for Hexavalent Chromium Adsorption: Equilibrium Mechanism, Kinetics, and Thermodynamics Analysis. *Groundw. Sustain. Dev.* **2022**, *18*, 100796. [CrossRef]
34. Tan, Y.; Wang, J.; Zhan, L.; Yang, H.; Gong, Y. Removal of Cr(VI) from Aqueous Solution Using Ball Mill Modified Biochar: Multivariate Modeling, Optimization and Experimental Study. *Sci. Rep.* **2024**, *14*, 4853. [CrossRef] [PubMed]
35. Liang, M.; Ding, Y.; Zhang, Q.; Wang, D.; Li, H.; Lu, L. Removal of Aqueous Cr(VI) by Magnetic Biochar Derived from Bagasse. *Sci. Rep.* **2020**, *10*, 21473. [CrossRef] [PubMed]
36. Fito, J.; Abewaa, M.; Nkambule, T. Magnetite-Impregnated Biochar of Parthenium Hysterophorus for Adsorption of Cr(VI) from Tannery Industrial Wastewater. *Appl. Water Sci.* **2023**, *13*, 78. [CrossRef]
37. Parameswari, E.; Kalaiarasi, R.; Davamani, V.; Kalaiselvi, P.; Paul Sebastian, S.; Suganya, K. Potential of Activated Biochar for Sequestration of Chromium (VI) from Aqueous Solution: Parameters Optimised by RSM, Isotherm and Kinetics Study. *Int. J. Environ. Anal. Chem.* **2023**, *103*, 6816–6834. [CrossRef]
38. Bayuo, J.; Abukari, M.A.; Pelig-Ba, K.B. Optimization Using Central Composite Design (CCD) of Response Surface Methodology (RSM) for Biosorption of Hexavalent Chromium from Aqueous Media. *Appl. Water Sci.* **2020**, *10*, 135. [CrossRef]

39. Ben Khalifa, E.; Rzig, B.; Chakroun, R.; Nouagui, H.; Hamrouni, B. Application of Response Surface Methodology for Chromium Removal by Adsorption on Low-Cost Biosorbent. *Chemom. Intell. Lab. Syst.* **2019**, *189*, 18–26. [CrossRef]
40. Soleimani, M.; Jamali, H.A.; Mousazadehgavan, M.; Ghanbari, R. Chromium Adsorption Using Powdered Leaves of Prosopis Cineraria: Kinetic, Isotherm, and Optimization by Response Surface Methodology. *Desalin. Water Treat.* **2024**, *317*, 100286. [CrossRef]

Disclaimer/Publisher's Note: The statements, opinions and data contained in all publications are solely those of the individual author(s) and contributor(s) and not of MDPI and/or the editor(s). MDPI and/or the editor(s) disclaim responsibility for any injury to people or property resulting from any ideas, methods, instructions or products referred to in the content.